Spin-density waves and reorientation effects in thin epitaxial Cr films covered with ferromagnetic and paramagnetic layers

P. Bödeker, A. Schreyer, and H. Zabel
Institut für Experimentalphysik/Festkörperphysik, Ruhr-Universität Bochum, D-44780 Bochum, Germany
(Received 11 September 1998)

We report about synchrotron and neutron-scattering studies investigating incommensurate spin-density waves (I-SDW's) in epitaxially grown thin Cr(001) films, including surface and interface effects. These studies show that thin ferromagnetic cap layers of Fe, Ni, and Co with a thickness of only 2–3 nm have a strong effect on the propagation and orientation of the I-SDW's in Cr. For thick Cr films there exist essentially only transverse I-SDW's propagating parallel to the film plane with the spins oriented normal to the plane and at right angles to the in-plane magnetization of the ferromagnetic cap layers. With decreasing Cr thickness a different transverse I-SDW grows at the expense of the in-plane ones, now propagating normal to the plane and with spins parallel or antiparallel to the film magnetization. At a Cr thickness of about 250 Å , the transverse out-of-plane I-SDW completely dominates the phase diagram of Cr. All other domains are suppressed and a spin-flip transition does not occur above 10 K in strong contrast to bulk. For in-plane propagation of the I-SDW we find a coexisting commensurate spin-density wave (C-SDW) which vanishes during the reorientation to out-of-plane propagation with Cr thickness. Finally, for Cr thicknesses well below the period of the I-SDW, the Cr can only order as a C-SDW. The behavior of the SDW's in thin Cr films with ferromagnetic cap layers can be understood in terms of competing interactions at the rough interfaces inducing frustration and by finite-size and strain effects. We have also investigated the effect of Cu and Pd cap layers on the SDW. The Cu cover is similar to a Cr/vacuum interface, whereas the effect of the Pd cover is intermediate between the ferromagnetic layers and Cu. [S0163-1829(99)11513-3]

I. INTRODUCTION

The complex magnetic structure of Cr, comprising an incommensurate antiferromagnetic spin-density wave (I-SDW), has been of continuing interest since its discovery in 1959.[1] Recent attention to the magnetic structure of Cr is in part due to its use as spacer layer in giant magnetic resistance materials, in particular in Fe/Cr (Refs. 2 and 3) and Co/Cr superlatttices.[4] Predictions of surface enhanced magnetic moments and topological ferromagnetic order on stepped Cr surfaces[5] have spurred much experimental activity using surface science methods to characterize the magnetic surface state of Cr.[6] However, a characterization of the Cr magnetic state at surfaces and in thin films is not an easy task. Frequently used experimental techniques in the area of surface and thin-film magnetism, such as vibrating sample magnetometry, superconducting quantum interference device magnetometry, or magneto-optical Kerr effect are only applicable to ferromagnets. In the past, the most powerful method for studying the magnetism of Cr has been neutron scattering due to its sensitivity to antiferromagnetism. On the other hand, when studying thin films, the intensity of neutron sources may not suffice. Nevertheless, we will show that neutron scattering remains the most useful and direct method even for thin-film investigations. With elastic magnetic neutron-diffraction the spin orientation and the propagation direction of the spin-density waves can be analyzed. Furthermore, commensurate and incommensurate SDW's can easily be distinguished and the magnetic moments including their orientation can be determined. Scattering with synchrotron x-ray radiation is a very important alternative to neutron scattering. With this method either the Thomson or the magnetic scattering cross section can be utilized. However, since no magnetic resonance enhancement occurs at the Cr K edge, the magnetic cross section is too weak for the investigation of thin films. The normal Thomson cross section yields information on the propagation of the charge-density (CDW's) and strain waves (SW's) accompanying the spin-density waves, but not on the orientation of the Cr spins. Recently, perturbed angular correlation spectroscopy (PACS) has been used for the analysis of SDW's in Cr films.[7,8] This method is only sensitive to the spin orientation but not to the propagation of the SDW's. In contrast to synchrotron charge scattering, PACS experiments can distinguish between commensurate and incommensurate SDW's and can provide an estimate for the magnetic moments. Compared to the other methods, neutron scattering remains the only experimental technique which provides information on both spin orientation and propagation direction of the spin-density waves, on commensurate and incommensurate phases, as well as on the magnetic moments. Examples of this will be shown further below.

For an excellent and comprehensive review of the physical properties of Cr we refer to the review paper by Fawcett.[9] Here, only the properties, which are of direct concern to this paper are briefly mentioned. Chromium has a bcc structure with a lattice parameter $a=2.88$ Å . As a $3d$ metal, Cr has to be considered an itinerant antiferromagnet with an average magnetic moment of $0.46\mu_B$ per atom at 4.2 K.[10] If Cr had a commensurate antiferromagnetic structure, the magnetic moment density at the corners would be opposite to the ones at the center of the bcc unit cell, as schematically indicated in Fig. 1(a), forming a commensurate spin-density wave (C-

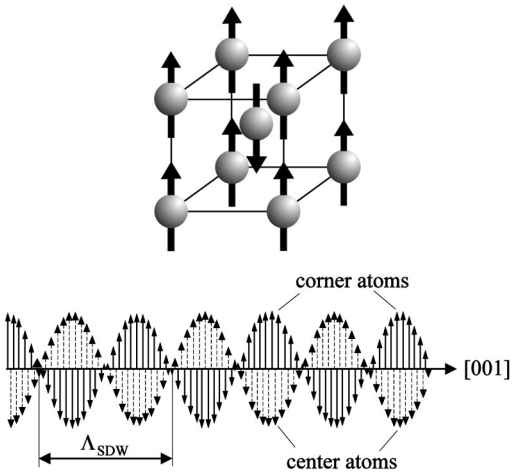

FIG. 1. Schematic representation of the magnetic structure of Cr. The top shows the bcc unit cell of Cr with the arrows indicating a commensurate antiferromagnetic spin structure. The lower panel represents the incommensurate modulation of the antiferromagnetic spin structure causing an incommensurate spin-density wave. Here a transverse I-SDW propagating in the [001] direction is shown with the magnetic moments at right angles to the propagation direction. Λ_{SDW} indicates the period of the I-SDW, which is about 42–54 Cr monolayers depending on temperature.

SDW) structure with a wave vector of $Q=2\pi/\Lambda=2\pi/a=2.18$ Å^{-1} commensurate with the lattice, where Λ is the periodicity of the *C*-SDW. Furthermore, the magnetic moments can be oriented parallel to any of the {100} crystallographic axes. Therefore, in thermal equilibrium three different domains are expected to coexist for the different orientations of the magnetic moments. Pure Cr exhibits, in fact, an incommensurate spin-density wave (I-SDW) structure, which consists of a sinusoidal modulation of the magnetic moments, as shown schematically for a transverse SDW in Fig. 1(b). Here the magnitude of the SDW wave vector is $Q=(2\pi/a)(1-\delta)=2\pi/a-2\pi/\Lambda_{SDW}$, where δ is a measure of the deviation from the commensurability and Λ_{SDW} is now the periodicty of the incommensurate SDW. The I-SDW can be visualized by a spin lattice which is slightly expanded as compared to the crystal lattice, yielding a beating effect between both, with a beat periodicity of $\Lambda_{SDW}=a/\delta$. In bulk Cr Λ_{SDW} increases smoothly from 60 Å at 10 K to 78 Å at the Néel temperature of 311 K, corresponding to an increase from 42 to 54 Cr monolayers, respectively.

Next we need to distinguish between the propagation direction and the orientation of the I-SDW. The propagation direction can be any of the three crystallographic {100} directions. The orientation may, however, be either longitudinal or transverse. For longitudinal I-SDW's the spins are oriented parallel to the propagation direction $\vec{Q},(\vec{S}||\vec{Q})$, whereas for the transverse I-SDW's they are oriented perpendicular to $\vec{Q},(\vec{S}\perp\vec{Q})$. In bulk Cr one finds at low temperatures a longitudinal I-SDW, refered to as the AF_2 phase. Usually all three propagation directions occur with equal probability in three different domains. At 123 K a first-order spin-flip transition occurs to a transverse I-SDW (AF_1 phase), again coexisting in different domains. The transverse I-SDW exhibits a first-order Néel transition at 311 K. Above 311 K, Cr is a paramagnet. Between 123 and 311 K the periodicity of the SDW depends markedly on the temperature, increasing from 60 Å at 123 K to 78 Å at 311 K, as mentioned before.

Under normal conditions, below the Néel temperature bulk Cr forms a polydomain state. A single domain state can, however, be achieved by cooling the sample through the Néel temperature either in a high external magnetic field or under tensile stress along one of the cube edges. As already pointed out, the spin-density-wave structure of Cr is usually incommensurate. However, elastic strains or chemical impurities may cause the SDW to be commensurate.[11] For instance, alloying 3% Mn is sufficient for a complete transition to the commensurate phase. The commensurate antiferromagnetic structure is designated as the AF_0 phase.

We have recently studied the spin-density-wave structure in thin epitaxial Cr(001) films as a function of film thickness and temperature[12,13]. Aside from a native oxide layer, these films were not covered by another metallic film. The striking features of these experiments include a single-$\vec{Q}$ longitudinal I-SDW, propagating out-of-plane, an enhanced modulation period of the magnetic moments, an enhanced spin-flip temperature, and a commensurate antiferromagnetic phase with moments out of plane, which first appears close to the bulk Néel temperature at 311 K and persists well above it. The enhanced Λ_{SDW} can be attributed to strain effects. Possible explanations for the out-of-plane propagation of the ISDW and the out-of-plane orientation of the Cr spins in our samples include surface pinning effects, hybridization with the buffer Nb layer, and interaction with the native Cr oxide layer at the surface. PACS experiments by Meerschaut *et al.* on one of the samples[8] agree with the presence of an incommensurate and a commensurate phase with spins oriented perpendicular to the surface. Unlike neutron scattering the PACS data also allows an independent determination of the relative volume fraction of both phases and the respective magnetic moments of the Cr atoms in both phases.

Here we report on neutron and synchrotron scattering experiments to study the effects that ferromagnetic and paramagnetic cap layers have on the SDW's in epitaxial Cr(001) films. These investigations are important for a better understanding of interface effects between ferro- and antiferromagnetic layers with possible applications to exchange coupling and interface bias effects. In particular for the Fe/Cr interface we know that the interlayer exchange integral is negative, prefering an antiparallel alignment of the Fe and Cr magnetic moments at the interface.[14] Thus, for a perfectly sharp interface we expect that a ferromagnetic Fe layer with in-plane magnetization will project out a transverse SDW propagating perpendicular to the plane with spins in the plane, as depicted in Fig. 23. Almost ideal epitaxial growth of Cr(001) on a Fe whisker appears to support this notion.[15,16] Domain images of a top Fe layer capping a Cr wedge on a Fe whisker substrate show that the average magnetization vector in the Fe domains rotates by 180°, whenever the Cr layer thickness is incremented by one monolayer. Additional phase slips are consistent with the incommensurability induced by an I-SDW.[16] However, interfacial roughness may have a dramatic effect on the orientation of the SDW's in the Cr films, on the domain formation of the SDW's, and possibly on the magnetic moments themselves.

Computer simulations by Stoeffler and Gautier[17] have shown that interfacial roughness may lead to a moment reduction. This appears to be supported by the Mössbauer experiments probing the hyperfine fields close to the Fe/Cr interface.[18]

In this paper we provide the first systematic study of spin-density waves in epitaxial Cr(001) films covered with ferromagnetic and paramagnetic cap layers as a function of the Cr film thickness. Preliminary reports of these studies[19,20] as well as a letter-style excerpt[21] have been published elsewhere.

This paper is organized as follows. In Sec. II we describe the scattering techniques used, including the selection rules for synchrotron and elastic magnetic neutron scattering, in Sec. III we provide information on the sample preparation and sample characterizations, in Sec. IV we discuss the experiments on SDW's in Cr films capped with Fe layers, in Sec. V we report about equivalent measurements with ferromagnetic cap layers of Co and Ni and with the paramagnetic layers of Cu and Pd. Finally in Sec. VI we discuss our results and compare the effect of the different cap layers on the SDW in epitaxial Cr(001) films. In closing we want to emphasize that this paper mainly deals with proximity effects between the SDW state in Cr films and ferromagnetic or paramagnetic cap layers. It does not discuss the interlayer exchange coupling which results from this. For the latter properties we refer the interested reader to recent reviews[22,23] and to a number of recent publications.[7,24–28]

II. SCATTERING EXPERIMENTS

The most powerful tool for the investigation of spin structures and phase transitions in Cr has been elastic neutron-neutron scattering.[29] More recently also x-ray and synchrotron scattering experiments have been added.[30–32,12,13] In neutron-scattering experiments the magnetic moment of the neutrons couple to the magnetic moments of the magnetic material via dipolar interaction. Working out the elastic-scattering cross section, one obtains[33,34] for the scattering cross section of an unpolarized neutron beam with a magnetization wave $\vec{M}(\vec{r})$:

$$\frac{d\sigma}{d\Omega}^{n} = |\vec{M}_q|^2 \sin^2\Theta_q , \tag{1}$$

where Θ_q is the angle between $\vec{M}$ and $\vec{q}$, and $\vec{M}_q$ is the Fourier component of $\vec{M}(\vec{r})$, corresponding to the scattering vector $\vec{q}=\vec{k}'-\vec{k}$. Equation (1) describes the scattering intensity of a Bragg peak due to a magnetization wave $\vec{M}(\vec{r})$, which in the case of Cr represents the SDW with a polarization vector $\vec{S}(\vec{r})=\vec{M}(\vec{r})$ and a spin-density-wave vector $\vec{Q}$.

Figure 2 shows a partial reciprocal lattice of Cr. The SDW satellite peaks are marked by open circles. They occur around the structurally forbidden bcc reflections. Any intensity in their vicinity has, therefore, to be of magnetic origin. There are two selection rules to be obeyed for finding the propagation direction and spin orientation of SDW's. First, the vector between any of the satellite peak positions and the next-nearest-allowed bcc reciprocal-lattice point determines the propagation direction of the SDW. Second, the magnetic neutron-scattering cross section yields only intensity for components of the magnetization vector perpendicular to the scattering vector. At least six scans along *H*, *K*, and *L* across the satellite peak positions at two different orthogonal reciprocal-lattice points are required for a unique characterization of the SDW's in Cr. For thin films the *z* axis is defined to be perpendicular to the film plane, i.e., *L* is the out-of-plane direction whereas *H* and *K* are the two equivalent in-plane directions. In practice, four scans across the (010) and (001) positions in the *K* and *L* directions, respectively, have turned out to be most useful for thin films, since the two in-plane directions *H* and *K* can be regarded as equivalent. In this case the scan directions are always either parallel or perpendicular to the scattering vector, which simplifies considerably the interpretation of the results. For example, scanning along the *K* direction across the (010) position will detect an in-plane transverse SDW with spins either parallel to *H* or *L*. Another *K* scan at the (001) position reveals whether there are any in-plane components of the Cr magnetic moments. If satellite peaks exist in this scan, the spins lie in the plane, otherwise they are orientated in the perpendicular direction. Table I provides a summary of the four different scan directions and their interpretation according to the selection rules.

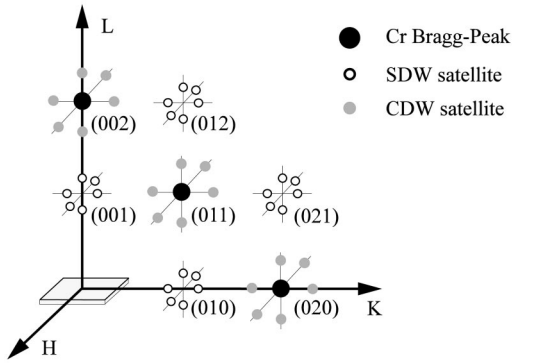

FIG. 2. Overview of the satellite reflections as they occur for different longitudinal and transverse incommensurate spin-density waves.

The magnetic spin-density-wave vector $\vec{Q}$ can also be measured via nonresonant magnetic x-ray scattering, as has recently been shown by Hill *et al.*[35] According to Brückel *et al.*,[36,37] the nonresonant magnetic x-ray cross section for very high photon energies ($\geqslant 100$ keV) can be written as

$$\frac{d\sigma}{d\Omega}^{\text{x-ray}} = r_0^2 \left(\frac{\lambda_C}{d}\right)^2 |S_\perp|^2 . \tag{2}$$

Here, r_o^2 is the classical electron radius, λ_C is the Compton wavelength, *d* is the interplanar lattice spacing, and $S_\perp$ is the spin component perpendicular to the scattering plane. Thus, nonresonant magnetic x-ray scattering with high-energy photons is sensitive to the spin component perpendicular to the scattering plane, and the selection rules are similar to those for magnetic neutron scattering. However, this scattering contribution is rather weak and can only be applied to bulk samples.[37] Resonant enhancement of the magnetic cross section does not occur in the vicinity of the Cr *K* edge. Therefore, magnetic x-ray scattering on Cr films remains not prac-

TABLE I. List of four different neutron scans across the (001) and (010) reflections used in the present work and the information gained from these scans. The schematics indicate the positions of the satellites in reciprocal space observed for each of the I-SDW's listed.

SDW Mode	(001) L-Satellite	(001) K-Satellite	(010) L-Satellite	(010) K-Satellite
out-of-plane longitudinal Spins out-of-plane	○	○	●	○
out-of-plane transversal Spins in-plane	●	○	●	○
in-plane longitudinal Spins in-plane	○	●	○	○
in-plane transversal Spins in-plane	○	●	○	●
in-plane transversal Spins out-of-plane	○	○	○	●
	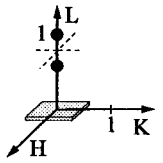	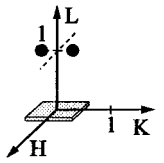	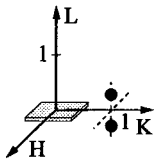	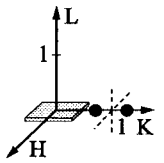

tical. The spin-density wave sets up a charge density and a strain wave in the Cr lattice. The amplitude of the charge-density wave is only about 0.1 electrons and can hardly be recognized in the presence of the normal charge scattering. The strain wave, on the other hand, is more easy to detect. The strain waves can be visualized as frozen phonons, yielding the same selection rule for the scattering cross section as a one-phonon cross section, i.e., the scattering vector and the displacement amplitude form a scalar product $(\vec{q}\cdot\vec{\Delta})$, where $|\vec{\Delta}|$ is the amplitude of the strain wave. Therefore, only satellite reflections with a $\vec{Q}$ component parallel to the scattering vector $\vec{q}$ will yield intensity, the others are silent. The charge-density wave and the strain wave are independent of the orientation of the magnetic moment. Therefore, the periodicity is only half that for the spin-density wave and the wave number is doubled. Thus, the satellite reflections due to the CDW or SW occur at the positions $\pm 2\vec{Q}$ close to the bcc allowed charge peaks at {200}, {110}, etc., providing information on the propagation direction of the spin-density waves but not on their polarization (see Fig. 2). For information on the spin direction and polarization, neutron scattering is required. Furthermore, with neutron scattering one can easily distinguish between commensurate and incommensurate SDW's, since at the {100} position no scattering from the chemical structure is allowed. In contrast, the huge allowed charge peak at the {200} position is prohibitive for detecting any commensurate phase with synchrotron experiments. Therefore, neutron scattering has a distinct advantage over synchrotron x-ray scattering as concerns the analysis of the polarization of the SDW and the detection of commensurate contributions. The disadvantage of neutron scattering is the lower flux even at high flux neutron sources as compared to synchrotron sources. Therefore, elastic neutron scattering for the study of SDW's in Cr films is limited to thicknesses down to about 1000 Å . Investigation of thinner Cr films requires the growth of multilayers, such that the signal can be added up from a stack of Cr layers.

We have carried out synchrotron experiments at the National Light Source in Brookhaven (NSLS, beamline X22B) and at the HASYLAB in Hamburg (beamline RÖWI). Neutron-scattering experiments were carried out at the research reactors of the National Institute of Standards and Technology (NIST, instrument BT2), and of the Forschungszentrum Jülich (instrument UNIDAS). In all cases we used a monochromater and analyzer. For the synchrotron experiments either two Si(111) crystals (HASYLAB) or two Ge(111) crystals (NSLS) were used. For the neutron experiments we used highly oriented pyrolytic graphite as monochromator and analyzer. The $\lambda/2$ contamination was suppressed with a stack of pyrolytic graphite filters.

III. SAMPLE DESIGN, GROWTH METHODS, AND CHARACTERIZATIONS

A. MBE growth

We have grown single crystalline bcc Cr[001] layers on $Al_2O_3[1\bar{1}02]$ substrates with a Nb[001] buffer layer using molecular-beam epitaxial (MBE) methods. Using a well established growth recipe already reported previously[12] we achieved high-quality single-crystal growth of the Cr films on the Nb buffer. The universal three-dimensional epitaxial relation between Nb and sapphire, which is essential for growing epitaxial metal films with single domains, has already been reported by Durbin *et al.*[38] The Nb[111] direction points along the *c* axis of the sapphire, whereas the [001] direction of Nb is parallel to the $Al_2O_3[1\bar{1}02]$ direction, being the surface normal of the sapphire *R* plane. Since bcc-Cr grows parallel to bcc-Nb in spite of the large lattice

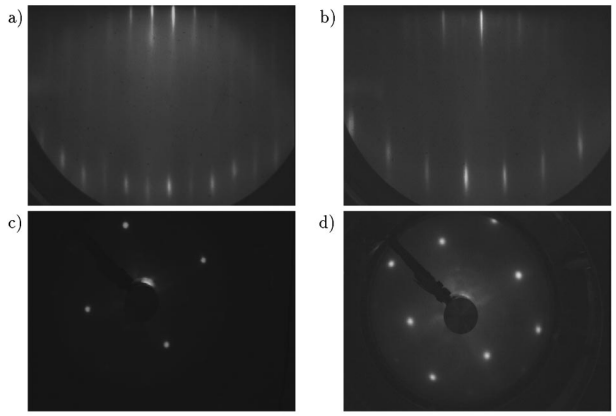

FIG. 3. RHEED and LEED pictures of the Cr(001) surface. (a) RHEED picture along the [100] azimuth, (b) along the [110] azimuth; (c) and (d) show the corresponding LEED pictures of the Cr surface.

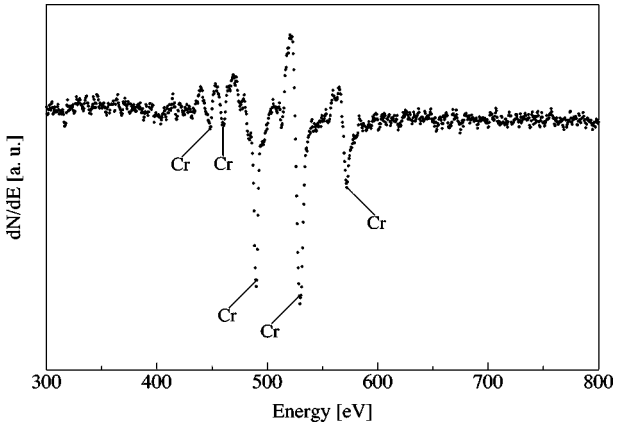

FIG. 4. Auger spectrum of the uncovered Cr surface of 2000 Å thick Cr film. No lines other than from Cr are visible.

mismatch of 13%, *R* plane orientated sapphire substrates are used for the growth of [001] oriented Cr films on Nb. We have grown a series of Cr layers with thicknesses ranging from 500 to 4000 Å as well as Fe/Cr(001) superlattices in this fashion. To maximize the amount of Cr in the beam, 5 $\times 5$ cm^2 large substrates were used for the samples intended for the neutron-scattering experiments. X-ray scattering and energy-dispersive x-ray spectra taken from the center and near the edges of the samples confirmed a perfect lateral homogeneity obtained by continuous rotation of the samples during growth. Due to the 13% lattice mismatch, pseudomorphic growth of Cr on Nb is excluded. As a result of the high lattice misfit the crystal quality of the first monolayers is not very high according to reflection high-energy electron diffraction (RHEED), but improves with increasing film thickness. We find that a minimal thickness of the Cr buffer of 200 Å is necessary for a sufficiently high film quality.[39] The Cr films are expanded in the film plane and relax with increasing film thickness.[40] The in-plane lattice relaxation follows the usual strain relaxation model for metals.[41]

The Cr(001) films were grown on Nb(001) at an optimized substrate temperature of 450 °C with a growth rate of 0.15 Å /s. At this temperature Cr(001) grows in a layer by layer fashion and there is essentially no increase of the surface roughness noticeable with increasing film thickness. After growth, the Cr films were annealed at 750 °C for 30 min, which leeds to a considerable improvement of the surface roughness and crystal structural coherence, as shown by the RHEED and low-energy electron diffraction (LEED) pictures presented in the next section.

After Cr growth and the annealing step, the samples were cooled to 300 °C and different 20 Å thick metal layers (M = Fe,Co,Ni,Cu,Pd) were deposited on the Cr. The growth temperature for the M layer is a compromise between surface roughness and interdiffusion. Finally, as a protection against oxidation, the M films were covered with another 20 Å thick Cr film. This Cr layer passivates the other epitaxial films since at room temperature and under normal atmospheric conditions the Cr-oxide film thickness saturates at about 10–15 Å .[42]

B. RHEED, LEED, and Auger analysis

Figure 3 shows RHEED and LEED pictures of the Cr surface in two different orientations after completion of the growth and after annealing. In both azimuths along the [100] and [110] direction, Laue zones of the zero and first-order reflections can be recognized. The LEED pictures are recorded with two different energies to probe the 100 (a) and the 110 surface symmetry (b). Figure 4 reproduces an Auger spectrum of the Cr surface after growth. Only the Cr LMM lines at 447, 459, 489, 529, and 571 eV are visible. There are no signs of any C, N, or O contaminations at the surface.

When depositing Fe on Cr, many RHEED oscillations can be observed. This is shown in Fig. 5.

A more detailed RHEED study of the growth of Fe(001) on Cr(001) as a function of substrate temperature and growth rate has been reported in Ref. 39. In Fig. 6 again RHEED and LEED pictures are reproduced after deposition of a 20 Å thick Fe cap layer on Cr. The sharp reflections seen in these graphs are an indication for the high quality of our samples. The Auger spectrum in Fig. 7 exhibits only Fe LMM lines at 562, 596, 651, and 703 eV, but no lines from the Cr sublayer, indicating that the Fe layer completely covers the Cr film. Furthermore, the lack of any O, N, or C lines proves again the chemical purity of the sample.

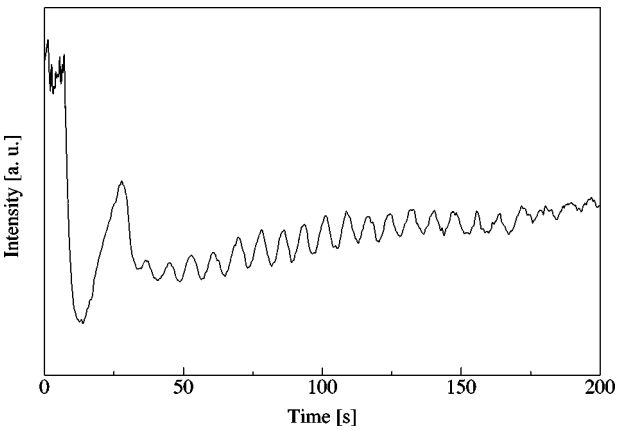

FIG. 5. RHEED intensity oscillations observed during the growth of Fe(001) on Cr(001).

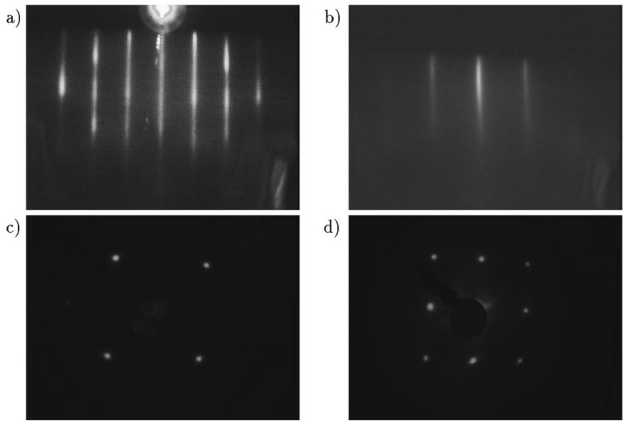

FIG. 6. RHEED and LEED pictures from the surface of a 20 Å thick Fe(001) layer on Cr(001). The top panels show RHEED pictures in the (a) [100] and (b) [110] azimuth. The lower panels show the corresponding LEED pictures of the Fe(001) surface.

C. X-ray characterization

We have characterized the structure of the Fe/Cr samples with our laboratory x-ray sources. Small-angle reflectivity measurements were used to determine the thicknesses of the individual layers. Figure 8 shows a typical example from a sample with a layer sequence starting from the top: 20 Å Cr/ 20 Å Fe/ 3300 Å Cr[001]/ 500 Å Nb/$Al_2O_3(1\bar{1}02)$. The short period oscillations, which are enlarged in the inset, are due to the Cr layer thickness. The longer period oscillations originate from the Nb buffer layer. Superimposed on these two oscillations is an even longer period oscillation with a broad maximum at 0.195 Å (Ref. 1) due to the 20 Å thick Fe cap layer and the 20 Å thick Cr of Cr-oxide protective layer.

Next we study the structural coherence length and the mosaicity of the Cr layers. In Fig. 9(a) a radial scan through the (002) Bragg peak of the same sample is shown as discussed before. The scan was performed using a Cu rotating anode source with a graphite monochromator in the incident beam. Due to the high structural coherence, the (002) peak is split in the two components originating from Cu $K\alpha 1$ and Cu $K\alpha 2$ radiation. The solid line represents a fit to the data points using three Gaussian peaks. Two of the Gaussian

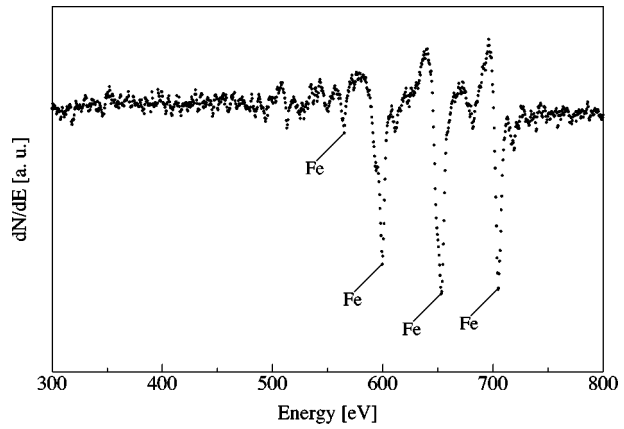

FIG. 7. Auger spectrum of the surface of the 20 Å thick Fe layer on Cr(001). Only Fe Auger lines are visible, but no Cr lines, indicating that the Fe layer completely covers the Cr surface.

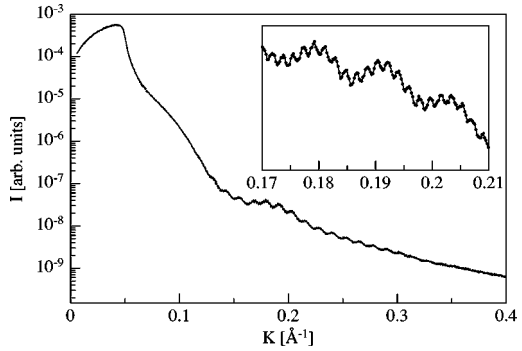

FIG. 8. Small-angle x-ray reflectivity scan of a sample consisting from surface to substrate of a 20 Å thick protecting Cr-oxide layer, 20 Å thick Fe(001) cap layer, 3300 Å thick Cr(001) film, 100 Å thick Nb(001) buffer layer on a $Al_2O_3(1\bar{1}02)$ substrate.

peaks describe the split peaks having a full width half maximum of $\Delta(2\theta)=0.062°$. This width translates into a structural coherence length of 1600 Å or about 50% of the total film thickness. The two peaks are superimposed on a broader weak peak with a width $\Delta(2\theta)=0.33°$. The broader peak most likely reflects some disorder at the Cr/Nb interface, where most of the structural relaxation takes place during growth. The scattering from the 20 Å thick Fe cap layer is completely submerged in this broader component. In Fig. 9(b) is shown a transverse scan through the Cr(002) reflection at the position of the $K\alpha 1$ peak. The solid line shows a fit to the data points with just one Gaussian peak with a width of $\theta=0.23°$. The anisotropy in the in- and out-of-plane coherence lengths will play an important role in explaining the origin of C-SDW's in the system.

We have also studied the in-plane structure and epitaxial relation of the Cr(001) using surface x-ray scattering methods under glancing incident and exit angles to the surface. Since we have reported earlier the epitaxial relation between Cr(001) and the Nb(001) buffer layer,[40] only the structural parameters will be discussed here. The in-plane structural coherence length for all samples reported in this paper lies between 250 and 350 Å , and the in-plane mosaicity is on the order of 0.3–0.4°. These values are slightly worse compared to the out-of-plane parameters for which we obtain coherence lengths of 50–80 % of the total film thickness and out-of-plane mosaicities of 0.2–0.3°.

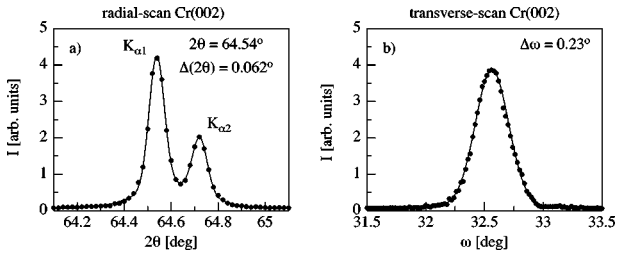

FIG. 9. (a): Radial x-ray scan through the Cr(002) reflection of a 3300 Å thick Cr film. The double peak is due to the indicent Cu radiation containing Cu-$K\alpha 1$ and Cu-$K\alpha 2$ spectral lines. The solid line is a fit to the data points with three Gaussian line shapes. (b): Transverse x-ray scan through the out-of-plane Cr(002) peak, measuring the mosaic distribution in the film. The solid line is a fit to the data points with one Gaussian line shape with a width of 0.23 degrees.

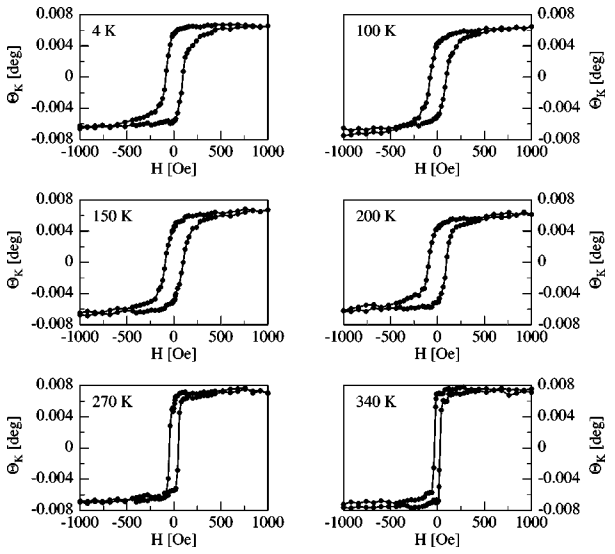

FIG. 10. Magnetic hysteresis curves of the 20 Å thick Fe cap layer on a 2100 Å thick Cr(001) film for different temperatures, measured with a high-resolution magneto-optical Kerr setup.

D. MOKE characterization

We have studied the magnetic properties of the overlayers via the magneto-optical Kerr effect (MOKE) using a setup described in more detail in Ref. 43. With a Faraday modulator and applying lock-in techniques we achieve an angular resolution of our Kerr magnetometer of better than 10^{-4} degrees. We used a He-Ne laser beam with a wavelength $\lambda = 632.8$ nm and a power of 5 mW. We have chosen the plane of polarization to be perpendicular to the plane of incidence (*s* state). We have investigated the longitudinal and polar Kerr effect over a temperature range from 4–340 K. In Fig. 10 longitudinal MOKE measurements from a 20 Å thick Fe(001) layer on a 2100 Å thick Cr film are reproduced for different temperatures. For the whole temperature range the easy axis remains in the plane. We do not observe a reorientation of the easy axis or a reduction of the order parameter over the temperature range investigated here. Therefore, we can safely assume that our 20 Å thick cap layers are in a ferromagnetic state with in-plane magnetization. This is also true for the Co and Ni layers. The shape of the hystereses curves in Fig. 10 changes with temperature. In particular the coercivity field increases with decreasing temperature which is due to the development of magnetic order in the Cr layers when going through the Néel temperature. This behavior is in basic agreement with the observations reported earlier by Berger and Hopster.[44]

IV. SDW IN CR FILMS CAPPED WITH FE LAYERS

A. Thick Cr films

1. Synchrotron radiation experiments

In Fig. 11 we reproduce scans with synchrotron radiation at 30 K for a 2100 Å thick Cr(001) film covered with a 20 Å Fe(001) layer. In order to determine the propagation direc-

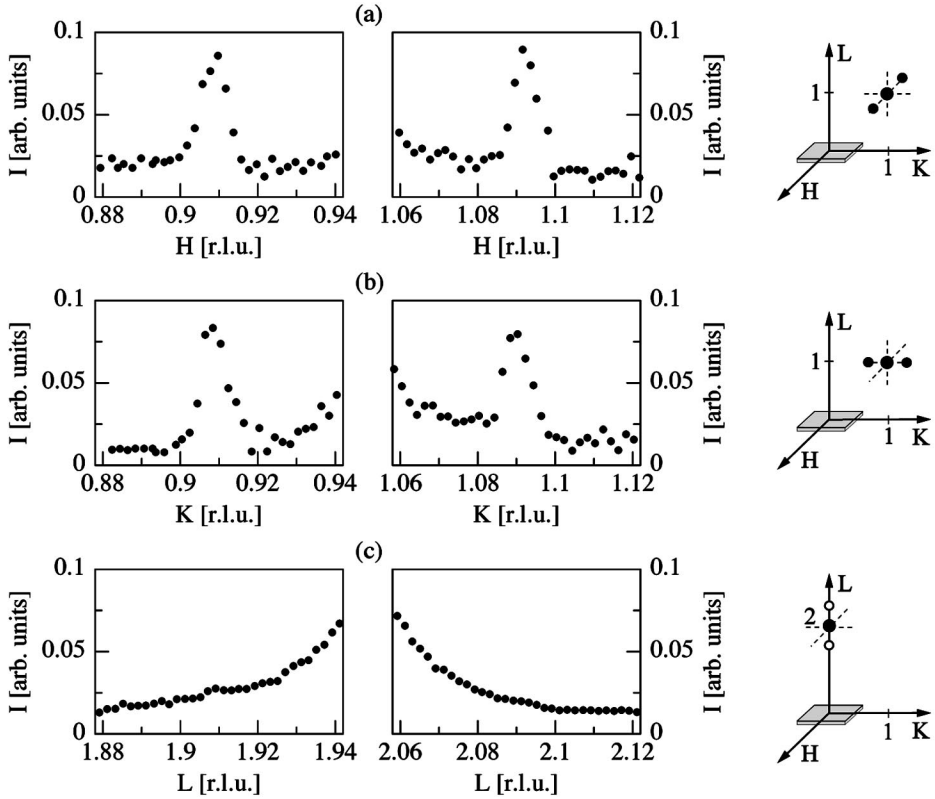

FIG. 11. Synchrotron measurement of the strain waves in a 2100 Å thick Cr(001) film capped with a 20 Å thick Fe layer. The scans were taken at 30 K. With three scans along the *H* direction (a), the *K* direction (b), and the *L* direction (c) the propagation direction of the strain wave can be uniquely determined. In this case the strain wave propagates entirely in the plane along the [100] and [010] directions, while the out-of-plane propagation is completely suppressed.

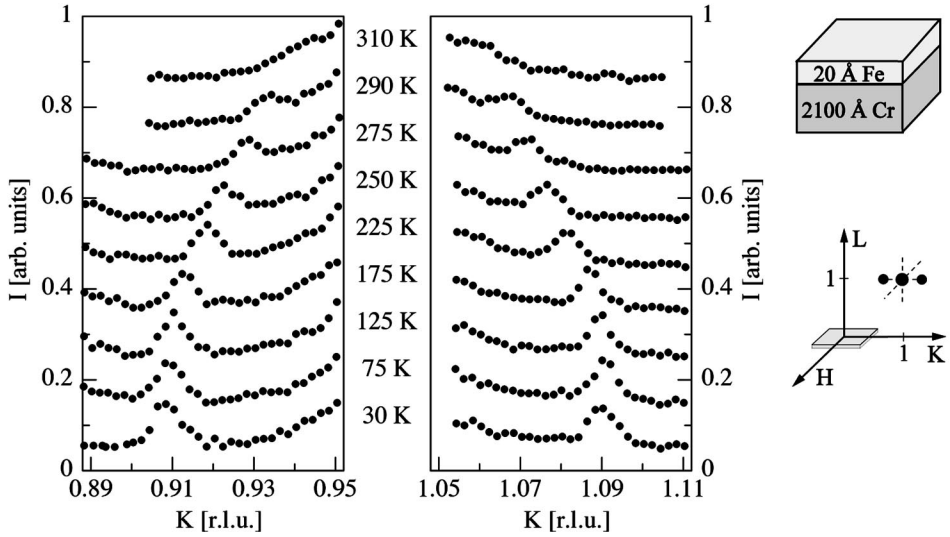

FIG. 12. Synchrotron data of the strain waves in 2100 Å thick Cr(001) film capped with a 20 Å thick Fe layer. Scans are recorded along the *K* direction across the (011) peak for different temperatures.

tions of the SDW, at least three scans have to be performed: two scans at the (011) reflection in the *K* and *H* direction to determine possible in-plane propagations, and one scan along the *L* direction at the (002) peak position to determine out-of-plane components. As can be seen by the scans presented in Fig. 11, CDW/SW satellite peaks exists only in the vicinity of the (011) peak position along the *H* and *K* directions. No satellite peaks are found at the (002) peak along the *L* direction. This implies that the SDW or CDW in this sample propagates only in the plane. Since the *H* and *K* satellites exhibit the same intensity, both propagation directions, along *H* and K, appear to be equally populated. There are no perpendicular components. From the width of the satellite peaks we determine a coherence length for the CDW/SW of about 300 Å . This is on the same order of magnitude as the in-plane structural coherence length of the Cr film, indicating that structural domains limit the coherence of the CDW/SW, not magnetic domains. Before we will determine the Cr spin orientation in relation to the propagation via neutron scattering, we first study the temperature dependence of the satellite peak intensity and of the peak position.

Scans at the (011) peak along the *K* direction are shown in Fig. 12 for different temperatures between 30 and 310 K. With increasing temperature the satellite intensity decreases continuously and the peak positions move smoothly towards the (011) commensurate position. From the peak position we can calculate the period of the CDW, which is plotted as a function of temperature in Fig. 13. Also shown is the temperature dependence for another thicker Cr film and for the bulk as reported by Werner *et al.*[29] The period of the CDW is enhanced in the thin films as compared to the bulk and scales inversely with the film thickness. An increased period for the CDW has already been noticed for plain Cr films and can be explained by residual epitaxial strains.[13]

The temperature dependence of the satellite peak intensity is shown in Fig. 14 for the two Cr films mentioned above, and these results are also compared with the intensities for bulk Cr measured with synchrotron radiation.[32] The dashed line denotes the peak intensity calculated in analogy to the BCS theory of superconductivity[45] yielding

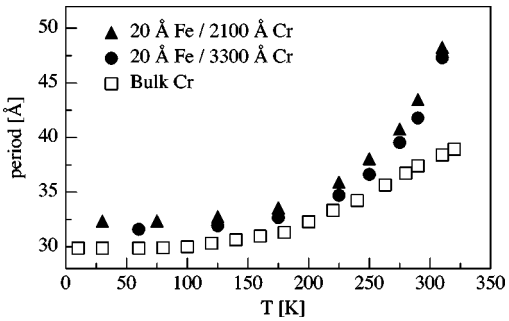

FIG. 13. Temperature dependence of the period of the strain waves in 2100 and 3300 Å thick Cr(001) films covered with a 20 Å thick Fe layer. The open squares indicate the temperature dependence of the period of the spin-density wave in bulk Cr, as determined by neutron scattering [from Werner *et al.* (Ref. 29)].

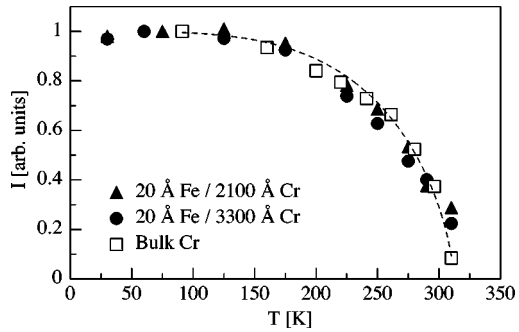

FIG. 14. Temperature dependence of the intensity of the strain wave satellite reflections as determined for the 2100 and 3300 Å thick Cr(001) films. The open squares show the corresponding measurements for bulk Cr [from Hill *et al.* (Ref. 32)]. The dashed line is a calculation of the intensity according to Eq. (3) with a Néel temperature T_N of 311 K. The intensity is normalized to 1 at 100 K.

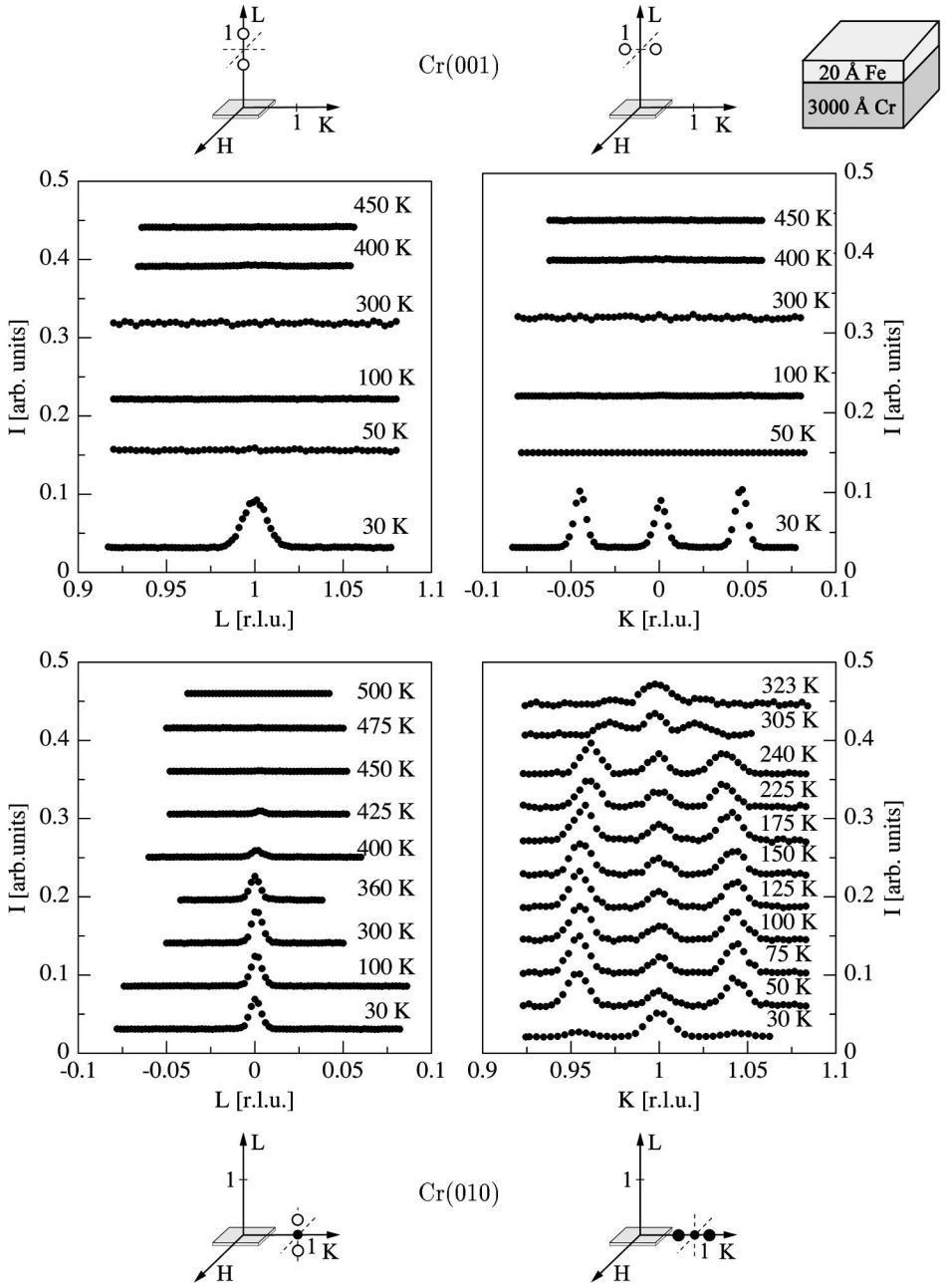

FIG. 15. Neutron scattering on a 3000 Å thick Cr(001) film covered with 20 Å thick Fe(001) layer to explore the the propagation directions and polarizations of the spin-density waves for different temperatures from 30 to 450 K. Scans are shown in different directions in the reciprocal space as sketched close to the respective panels, where the filled circles represent existing peaks while open circles indicate satellite positions scanned but no intensity detected at 50 K. For more details see text.

$$\frac{I(T)}{I(0)} = \left[1 - \left(\frac{T}{T_N}\right)^4\right]^{1/2}, \tag{3}$$

using the bulk Néel temperature $T_N = 311$ K. For most of the temperature range the satellite intensities from the epitaxial films match those of the bulk. Only close to the Néel temperature may some deviation to higher values be present. However, since the peak intensities close to T_N are very low, it is difficult to judge whether or not the Néel temperature in the thin films deviates from the bulk. Using the relation between external pressure and Néel temperature $T_N = -6.0$ kbar$^{-1} \times p + 311$ K,[46] and the pressure $p = -13.5 \pm 6$ kbar induced by the epitaxy, we would expect a Néel temperature of 389 ± 36 K for a 3000 Å film.[13] This value appears to be somewhat above the experimental result.

We have also varied the thickness of the Fe cap layers from 8 to 100 Å , keeping the Cr thickness nearly constant at a value of 2000 Å . In all cases the SDW propagates in the plane and the period of the CDW is again enhanced by the same amount. This shows that the Cr properties observed are due to the Fe/Cr interface and do not scale with the thickness of the ferromagnetic cap layer. Therefore, in the following experiments the thickness of the ferromagnetic cap layers was kept constant at about 20 to 30 Å . This thickness assures that the layers are homogeneously magnetized and do not break up into small domains. The Curie temperature of

the Fe, Co, and Ni layers is also sufficiently high such that they do not interfere with the Néel state of the Cr layer. The MOKE measurements discussed in Sec. III D confirm the ferromagnetic state of these cap layers.

2. Neutron scattering

In Fig. 15 we show the neutron results for a similar, 3000 Å thick Cr(001) film covered with 20 Å thick Fe layer, as used previously for the synchrotron experiments. The reason for using a slightly different sample is the larger surface area required for performing neutron-scattering experiments as compared to x-ray scattering. Figure 15 shows all four scan directions described before for different temperatures. The scans are offset by constant amounts for clarity. Above or below each set of scans the scan directions are shown. Open circles refer to satellite reflections which are allowed by the selection rules but not detected in the scans at 100 K, while closed circles refer to allowed *and* detected satellite reflections.

From 50 K up to about 311 K, satellite reflections due to incommensurate SDW's occur only in the K direction in the vicinity of the (010) position, i.e., at $(0,1\pm\delta,0)$. This confirms the synchrotron results that the incommensurate SDW propagates parallel to the film plane. This result, combined with the absence of satellites in the scan along K through (001) determines the spin orientation to be perpendicular to the film plane. On the other hand, at 30 K we observe large intensities for $(0,\pm\delta,1)$ satellites, while there are only weak satellite intensites at the $(0,1\pm\delta,0)$ positions. Again applying the selection rules described in Sec. II, this indicates a spin-flip transition between 30 and 50 K from a longitudinal to a transverse SDW, both propagating in the plane along K but with spins rotating from in-plane (below 40 ± 10 K) to perpendicular to the growth plane (above 40 ± 10 K). In the bulk, the spin-flip transition occurs at 123 K, whereas in the present thin film the transition is reduced to 40 ± 10 K. This spin-flip transition could not be detected with synchrotron scattering and is only seen by neutron scattering.

In addition to the incommensurate state, a commensurate antiferromagnetic spin strucure coexists starting from the lowest temperature to temperatures of at least 425 K, well above the Néel temperature for the incommensurate phase. At 30 K, the commmensurate (010) and (001) peaks indicate a C-SDW with spins oriented in-plane. Above the spin-flip transition at 40 ± 10 K, only the (010) peak remains, consistent with a C-SDW with spins out-of-plane. Thus, we observe a reorientation of the C-SDW at the spin-flip temperature of the coexisting I-SDW. Again, with synchroton scattering the commensurate phase could not be revealed. The origin of the C-SDW will be discussed below in Sec. VI.

A qualitative phase diagram for the 3000 Å thick Cr(001) film capped with a 20 Å Fe layer as derived from the neutron-scattering experiments is shown in Fig. 16. The relative volume fraction of the different phases was estimated from the intensity of the incommensurate satellite or commensurate Bragg reflections. At 30 K the sum of all intensities was set to 100%. Since the in-plane SDW can propagate along the [100] and [010] directions, their weight is counted twice.

While the phase diagram expresses relative intensities of the different coexisting phases and therefore shows the temperature dependence of the order parameters for the commensurate and incommensurate phases, it should not be concluded that the paramagnetic phase coexists with the incommensurate spin-density wave phase below the Néel temperature. As in all ferro- or antiferromagnetic systems the long-range order (or order parameter) becomes reduced with increasing temperature due to spin-wave excitations. Nevertheless, this does not imply a coexistence between paramagnetic and spin density wave phases below T_N. The paramagnetic phase with short range order exists only for $T\geqslant T_N$. However, above the Néel temperature of the incommensurate phase, commensurate and paramagnetic phases may indeed coexist.

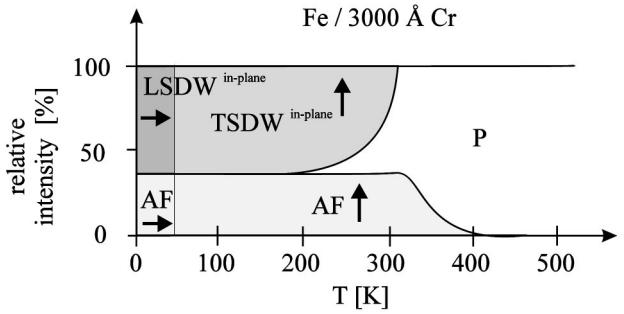

FIG. 16. Qualitative phase diagram for the spin-density waves in 3000 Å thick Cr(001) covered with a 20 Å thick Fe film, according to the results of the neutron-scattering experiments shown in Fig. 15. The arrows indicate the orientation of the magnetic moments in the respective phases, where the vertical direction refers to the [001] direction. LSDW and TSDW refers to the longitudinal and transverse incommensurate spin-density waves, respectively, AF indicates a commensurate phase and P the paramagnetic phase. The small labels ''in-plane'' and ''out-of-plane'' refer to the propagation direction of the I-SDW's.

The most remarkable result of these measurements is the fact that above the spin-flip transition and contrary to our expectations, the SDW's propagate in the film plane having their magnetic moments oriented perpendicular to the surface, i.e., at right angles to the Fe magnetization. This rather unexpected result signifies some roughness at the Fe/Cr interface causing frustration in the *inter*- and *intra*layer interaction. This will be discussed in more detail in Sec. VI.

B. 3000 Å thick Cr films sandwiched between Fe layers

Next we present results on the SDW's in a sandwich structure of 20 Å Fe/ 3000 Å Cr/20 Å Fe, i.e., without a Cr/Nb interface as in the sample discussed in the previous paragraph. This experiment allows us to study the significance of the Cr/Nb interface for the magnetic phase diagram. First we should note that the growth of Cr on Fe does not have the same high structural quality as the growth of Fe on Cr. This may lead to a broadening of the Bragg peaks. Second, two Fe/Cr interfaces on either side of a 3000 Å film may be viewed as equivalent to a 1500 Å thick Cr layer with just one Fe/Cr interface.

In Fig. 17 the neutron results from this sandwich structure are reproduced. Only scans along the $(0,\pm\delta,1)$ and $(0,1\pm\delta,0)$ positions are shown, the scans along L exhibit no structure at all and are therefore omitted. Starting from the

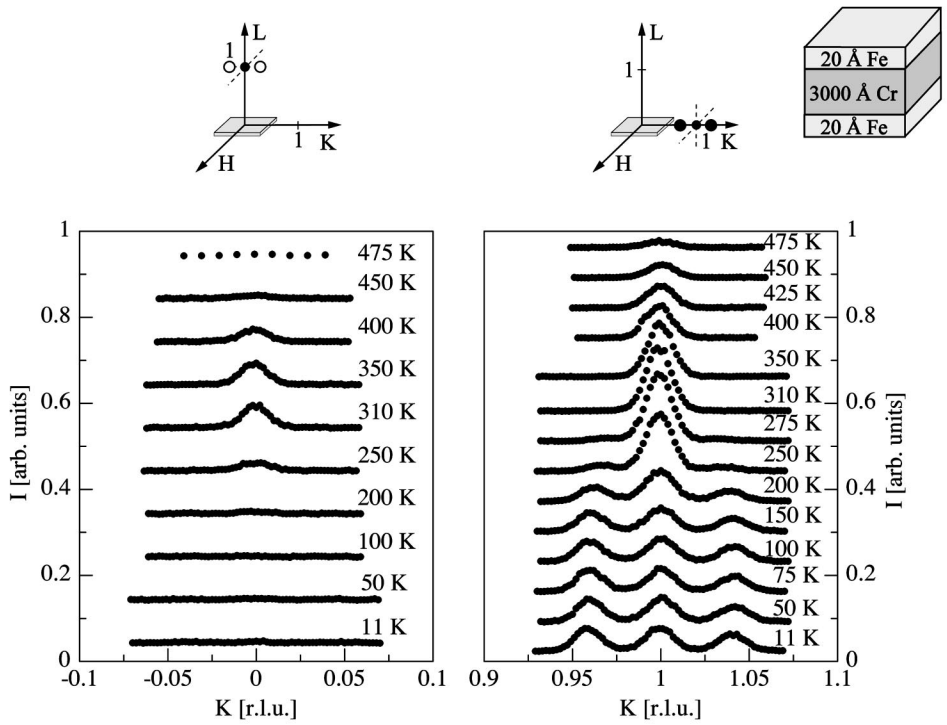

FIG. 17. Neutron-scattering experiments to explore the spin-density waves in a 3000 Å thick Cr(001) film sandwiched between 20 Å thick Fe layers on both sides as function of temperature. The scans show that the incommensurate spin-density wave propagates in the film plane and that the spins are oriented out-of-plane. A commensurate phase coexists from the lowest temperature of 11 K up temperatures far above the Néel temperature for the incommensurate phase.

lowest temperature of 11 K, there is a very pronounced I-SDW, propagating in the plane with spins out-of-plane, similar to the situation which we have seen before. This incommensurate phase is present from the lowest temperature measured up to the I-SDW Néel temperature. At the same time a commensurate phase coexists with the incommensurate phase exhibiting the same spin orientation. There is no spin flip transition observable above 11 K. The commensurate phase persists again to temperatures at least as high as 475 K. Interestingly, there is a second commensurate phase which occurs at about 200 to 250 K with spins oriented in-plane. As we will see below, it is important to note that this additional C-SDW occurs in the same temperature range in which the I-SDW vanishes. The phase diagram summarizing the volume fractions of the different phases as a function of temperature is reproduced in Fig. 18.

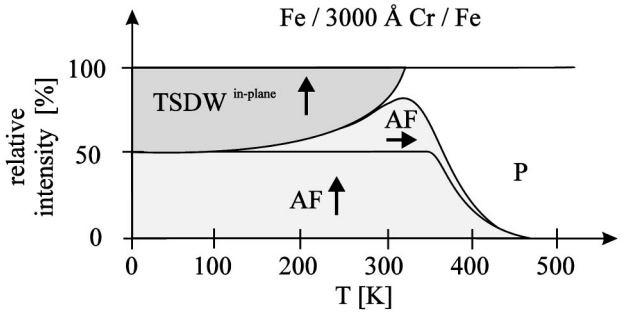

FIG. 18. Qualitative phase diagram for the commensurate and incommensurate spin-density waves in a 3000 Å thick Cr(001) sandwiched between 20 Å thick Fe layers, as derived from the neutron scans shown in Fig. 17.

C. 500 Å thick Cr layers

We will now reduce the Cr thickness further and study the phase diagram of the SDW's in 500 Å thick epitaxial Cr(001) films. The neutron data are collected from a superlattice comprising five double layers of [20 Å Fe/500 Å Cr]. As mentioned previously this was done to provide enough Cr in the experiment. The neutron results are shown in Fig. 19. The remarkable feature of these scattering data is the fact that now satellite reflections from the incommensurate phase occur in the K scans as well as in the L scans. While the scans shown in the lower right corner reflect the same behavior as before, a transverse I-SDW propagating out of the plane and with spins in the plane is clearly visible via the $(0,0,1\pm\delta)$ and $(0,1,\pm\delta)$ satellite peaks. Therefore, in this thickness range we have a mixture of in- and out-of-plane propagating I-SDW's. The commensurate phase coexists throughout the temperature range studied. At low temperatures the spins of the C-SDW lie in planes perpendicular to the growth direction. At 200–250 K again a second commensurate phase occurs with spins in-plane and parallel to the surface, reminiscent of the C-SDW observed before in the 3000 Å thick Cr film sandwiched between Fe. Again, there is no spin-flip transition above 15 K. All I-SDW's have a transverse nature. We should also note that the peaks in both commensurate and incommensurate phases are considerably broader than measured before, indicating shorter coherence lengths and more disorder in the spin lattice. This is

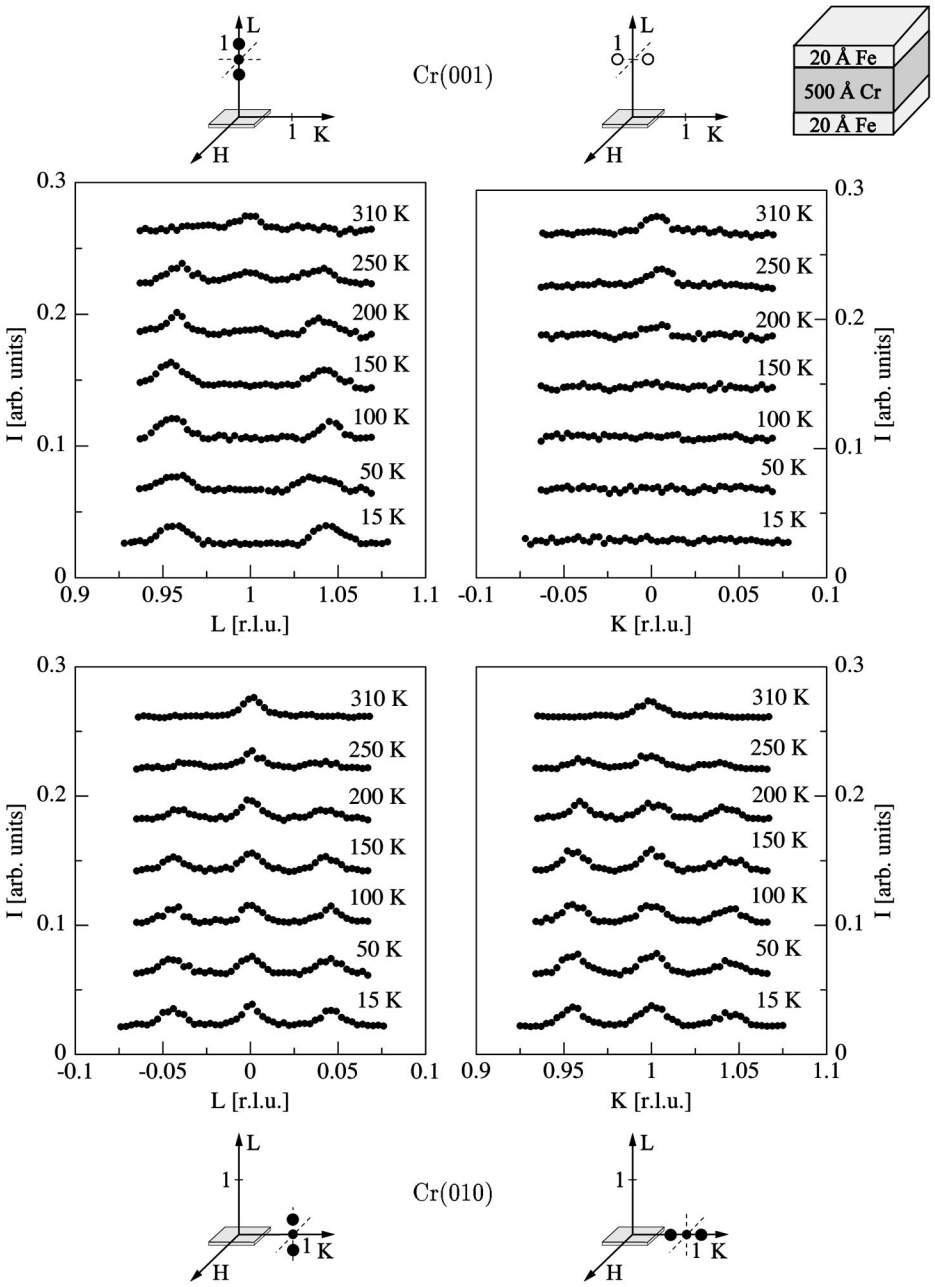

FIG. 19. Neutron scans similar to those shown in Fig. 15, now for a 500 Å thick Cr(001) film sandwiched between 20 Å thick Fe layers. In these scans a mixture of in- and out-of-plane transverse spin-density waves can be recognized.

probably the result of the poly-$\vec{Q}$ domain state with rather small domains for each individual $\vec{Q}$ state.

Unfortunately, for this sample no data for temperatures above 310 K are available. However, we assume that also here the volume fraction of the AF_0 phase has a maximum at about 350 K.

The phase diagram for the present sample is shown in Fig. 20. The most remarkable feature of this phase diagram is the fact that two instead of one transverse SDW with about equal volume fractions coexist. This indicates a reorientation of the SDW from propagating out-of-plane to in-plane, a reorientation, which will continued as we decrease the thickness of the Cr films.

D. 250 Å thick Cr film

We will now discuss the SDW's in a sample consisting of 10 double layers of [20 Å Fe/250 Å Cr]. The neutron scattering results are compiled in Fig. 21. For this sample we observe only a transverse SDW (T-SDW) propagating out of the plane with spins in the plane. There are only $(0,0,1\pm\delta)$ and $(0,1,\pm\delta)$ satellite reflections visible, all other satellite reflections have vanished. Therefore, the partial reorientation, which was already noticeable in the last sample, is completed here. It is also interesting to remark that the intensity of the $(0,0,1\pm\delta)$ satellites is due to T-SDW's domains with spins oriented along either the H or K direction. On the other hand, the $(0,1,\pm\delta)$ peaks are sensitive to the

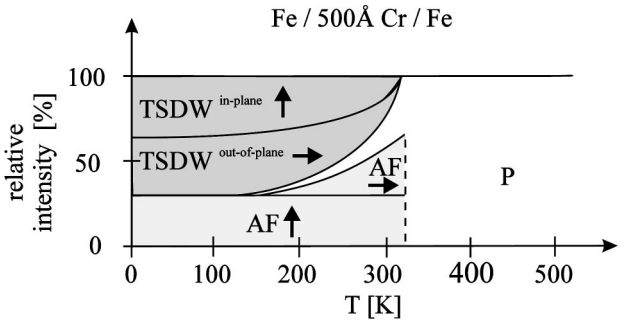

FIG. 20. Qualitative phase diagram for the commensurate and incommensurate spin-density waves in a 500 Å thick Cr(001) sandwiched between 20 Å thick Fe layers, as derived from the neutron scans shown in Fig. 19. The arrows indicate the orientation of the Cr spins in the different phases, where the vertical direction corresponds to the [001] direction.

same T-SDW but with spins oriented only along the *H* direction. These two sets of satellite peaks exhibit a 2:1 intensity ratio, indicating that indeed the propagation of the T-SDW is purely out-of-plane, and that each domain with spins oriented along the *H* and *K* direction occupies about the same volume fraction. The Néel temperature for the incommensurate phase is again close to 310 K, as seen previously.

In contrast to the samples studied before, there exists no commensurate phase at low temperatures. The C-SDW only becomes visible at higher temperatures when the I-SDW vanishes. In the commensurate phase the spins are also oriented parallel to the film plane. The phase transition for the commensurate phase is presumably again between 400 and 450 K, i.e., much higher than the Néel temperature of the incommensurate phase.

The phase diagram for this sample is shown in Fig. 22. It is much simpler than the phase diagrams for the thicker samples. Only one T-SDW propagating in the out-of-plane direction is seen which is the expected propagation and orientation of the SDW for a well-ordered Fe/Cr system. This situation is shown schematically in Fig. 23.

As we decrease further the thickness of the Cr layer, properties connected with the exchange coupling between the Fe layers become important. Our results have been discussed previously in detail by Schreyer *et al.*[24,27] and will not be dealt with here. Related work by Fullerton *et al.*[25,26] should also be noted. One important property of thinner Cr films not further investigated here is the thickness-dependent reduction of the Néel temperature for the incommensurate phase.[26,27] Finally, at a thickness of less than 45 Å an incommensurate spin-density wave cannot be established anymore at any temperature and T_N becomes zero. In this thickness range the Cr spin structure is completely commensurate antiferromagnetic and becomes strongly affected by lateral thickness fluctuations inducing a spiral Cr spin structure and strong noncollinear coupling between the Fe layers.[27]

V. CR(001) FILMS COVERED WITH CO, NI, CU, AND PD

The foregoing experiments have demonstrated that a 20 Å thick Fe layer has a dramatic effect on the SDW state of Cr. The proximity of Cr with other ferromagnetic, ferrimagnetic, or paramagnetic films would also be of high interest, however, much less is known on this subject at the present time. For example, reports on SDW's in Cr in proximity with Sn (Ref. 47) and Ag (Ref. 48) have been published recently. Nevertheless, none of these considered SDW's in thick Cr films. Here, we present the effect of thin ferromagnetic Co and Ni layers, as well as of paramagnetic Pd and Cu layers on the spin-density waves in thick Cr films. We discuss synchrotron and neutron-scattering results for roughly constant Cr layer thickness of about 2000 Å covered with the different ferromagnetic and paramagnetic layers.

A. Co cover

The Co/Cr(001) interface has attracted much less attention in the past than the Fe/Cr interface. It is, nevertheless, of considerable interest to compare these two interfaces as concerns their *interlayer*-exchange coupling and proximity effects on the SDW's in Cr. The somewhat lower interest in Co/Cr is, in part, due to the mismatched crystal structures and to the complex epitaxial relation between Co and Cr. While both Fe and Cr have a bcc structure with a lattice mismatch of less than 0.4%, the equilibrium crystal structure of Co is hcp. The first few monolayers of Co grow with a pseudomorphic bcc structure on Cr(001), where the original hcp *c* axis lies in the film plane and is rotated by a constant angle of 45° with respect to the Cr[100] in-plane axis. With increasing Co thickness the structure continuously relaxes back into the intrinsic hcp structure, while keeping the hexagonal *c* axis in the plane.[49–51] This lattice relaxation strongly affects the magnetic anisotropy properties at the Co/Cr interface.[52,43] Co on Cr exhibits a reorientational perpendicular anisotropy.[43] At a Co thickness of about 10 Å the easy axis rotates out of the plane but relaxes back into the plane with decreasing Co thickness. This reorientation is due to the concomitant structural phase transition of Co from hcp to pseudo-bcc. Here we work with Co thicknesses of 20 Å and more. Thus the Co film is almost completely relaxed to the hcp structure and displays an in-plane easy axis.

In Fig. 24 we show synchrotron results from a sample consisting of 2300 Å Cr(001) covered with a 20 Å Co layer. In the lower panel we reproduce *K* scans across the Cr(011) reflection for different temperatures, in the upper panel an *L* scan at 15 K across the Cr(002) reflection. *L* scans at other temperatures are omitted, since they are identical. Similar to the Fe/Cr case of comparable Cr thickness (compare Fig. 12), we find in-plane propagation of the CDW/SW for all temperatures. Compared to the Fe/Cr case, the satellite reflections appear broader, reflecting a shorter coherence length for the CDW/SW in Co/Cr and more disorder in the Cr spin lattice.

In Fig. 25 the equivalent neutron results are shown. For these measurements a different and larger sample was necessary, such that the thicknesses are not identical. This should, however, not affect the main conclusions. The I-SDW's and C-SDW's are almost completely identical to the case which we have discussed before for a 3000 Å Cr(001) film covered with Fe (compare Fig. 15). In particular, a spin-flip transition occurs close to 50 K. There is only one slight difference, as can be seen in the lower left panel of Fig. 25. Above the spin flip transition there exists a small

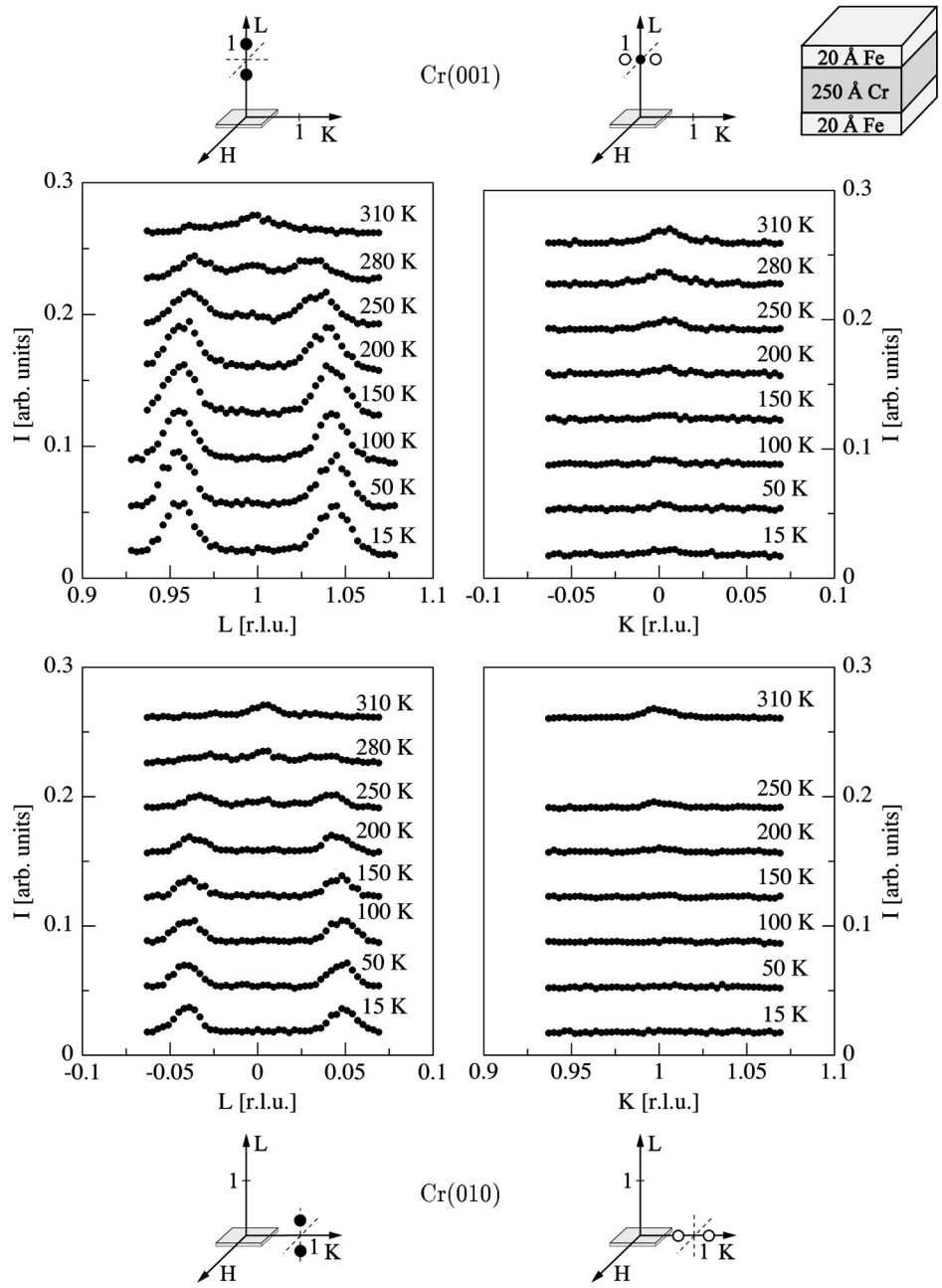

FIG. 21. Neutron scans similar to those shown in Fig. 15, now for 250 Å thick Cr(001) films sandwiched between 20 Å thick Fe layers. In these scans we can clearly recognize that the incommensurate spin-density waves propagates solely out-of-plane. No commensurate antiferromagnetic structure exists at low temperatue, only above the Néel temperature for the incommensurate phase.

fraction of a L-SDW propagating in the out-of-plane direction, which coexists with the much more dominant T-SDW, propagating in the film plane.

Combining the x-ray and neutron results, the phase diagram for this sample is shown in Fig. 26. Because of technical reasons, data above 300 K are not available. However, we assume from the experience with similar systems that the commensurate phase again persists up to about 400–500 K.

B. Ni cover

Similar synchrotron and neutron data for Cr(001) films covered with a 20 Å Ni layer are shown in Figs. 27 and 28. The scans again show a similar behavior for the SDW as seen before for Fe and Co cap layers. Note, however, that for this magnetic film the spin-flip transition is quenched at least to temperatures below 30 K. Therefore, the phase diagram is simpler, consisting only of a T-SDW with in-plane propagation and a commensurate SDW with spins out-of-plane.

C. Cu cover

Compared to the previous discussions, the effect of a 20 Å thick Cu layer on the phase diagram of 2000 Å Cr(001) is completely different. In Fig. 29 characteristic neutron scans from this sample are shown. The lower left panel confirms a

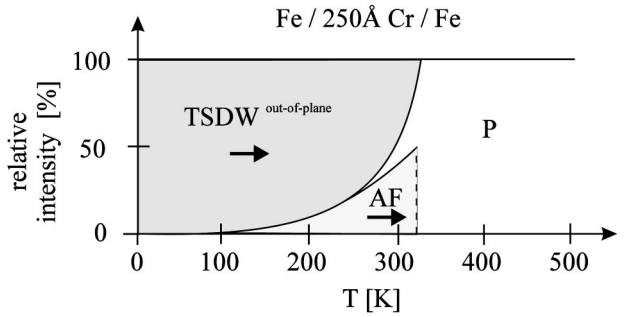

FIG. 22. Qualitative phase diagram for the commensurate and incommensurate spin-density waves in 250 Å thick Cr(001) films sandwiched between 20 Å thick Fe layers, as derived from the neutron scans shown in Fig. 21. The arrows indicate the orientation of the Cr spins in the different phases. As compared to the phase diagrams shown previously, this one is much simpler consisting only of one dominating transverse spin-density wave at low temperatures, with spins in the plane and propagation out-of-plane.

L-SDW propagating out-of-plane for all temperatures starting at 15 K up to the Néel temperature. Therefore, there is no spin-flip transition in this system. Second, there is no commensurate phase at low temperatures coexisting with the incommensurate SDW's as seen for the ferromagnetic cap layers. The commensurate phase occurs first close to the Néel temperature. A small amount of a T-SDW propagating in the out-of-plane direction starts at about 100 K, but remains a small fraction of the total volume. The phase diagram for this sample is shown in Fig. 30.

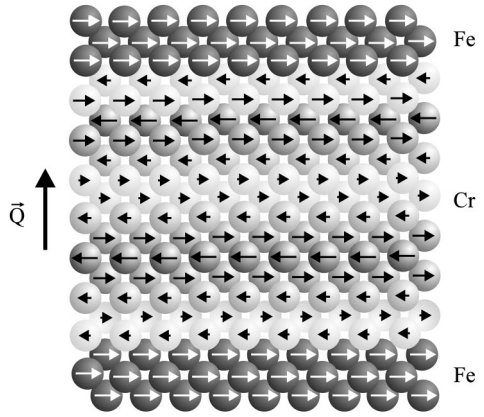

FIG. 23. Schematic representation of the magnetic structure depicted for the situation present in 250 Å thick films in proximity with Fe layers. The incommensurate spin-density wave propagates in the out-of-plane direction and the Cr spins are oriented in the plane, allowing for an antiferromagnetic exchange interaction at the Fe/Cr interface.

D. Pd cover

Finally we discuss the case of Pd on Cr(001). Pd is a highly polarizable metal with a Stoner enhancement factor of 9.3.[53] Therefore, we expect a considerable interaction between Pd and the top Cr layer. In fact, for monolayers of Cr on Pd(001), a strong enhancement of the Cr magnetic moment has been predicted.[54] Here we are not concerned with the magnetic moments at the Cr/Pd interface, however the mutual influence is appreciable, as revealed by our experiments.

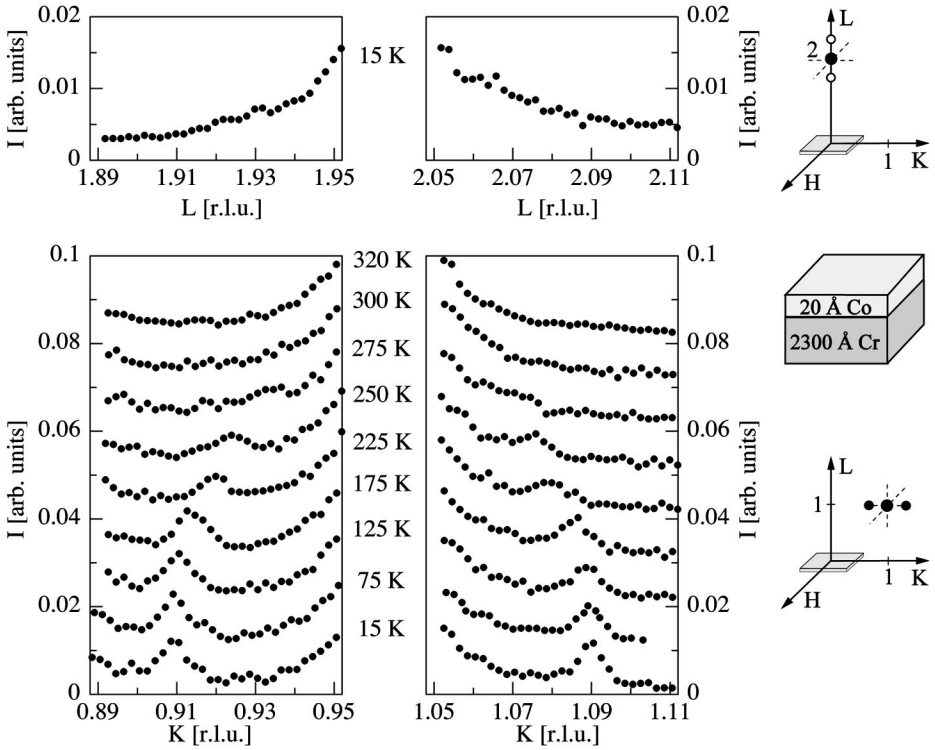

FIG. 24. Synchrotron measurements of the strain waves in a 2300 Å thick Cr(001) film covered with a 20 Å thick Co layer. Similar to the Fe covered thick Cr films, the strain wave propagates in the film plane.

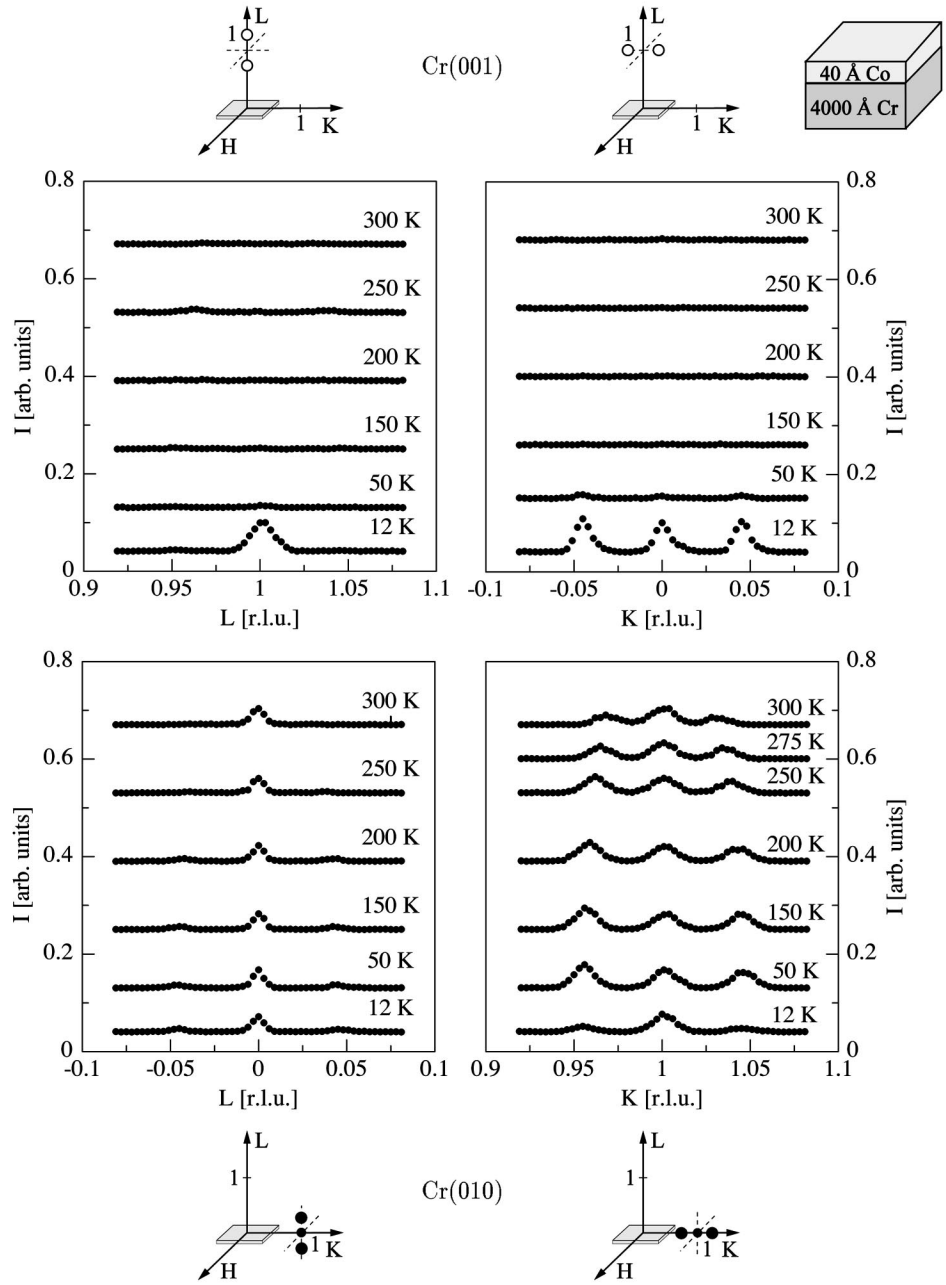

FIG. 25. Neutron-scattering experiments to explore the spin density waves in a 4000 Å thick Cr(001) film covered with a 40 Å thick Co layer for temperatures between 12 K and 300 K. Similar to the Fe covered thick Cr films, the incommensurate spin-density wave propagates in the film plane with spins oriented out-of-plane. Again a commensurate phase coexists from the lowest temperature of 12 K all the way up to 300 K.

In Figs. 31 and 32 are shown the x-ray and neutron-scattering results for a 2000 Å thick Cr film capped with a 30 Å thick Pd film. At low temperatures, three phases coexist, an in-plane T-SDW, an out-of-plane L-SDW and a minor fraction of a C-SDW. The minority commensurate phase becomes more dominant at higher temperatures with a maximum at about 300 K, and finally disappears above 400 K. In all three phases the Cr spins point out-of-plane parallel to the film normal. According to the intensities we estimate that the L-SDW phase occupies about 40% of the sample volume and is, therefore, the majority phase at low temperatures.

Comparing the Pd/Cr data with the previous examples it appears that the Pd effect on the SDW in Cr lies somewhere between Fe and Cu. In Fe/Cr the incommensurate SDW is only in-plane transverse, whereas in Cu/Cr it is only out-of-plane longitudinal. In Pd/Cr we see a mixture of both. The high magnetic polarizability of Pd appears to be able to rotate, at least partially, the SDW from out-of-plane to in-plane. Note that the fraction of commensurate phase at low temperatures is connected with the fraction of the in-plane propagating T-SDW.

There is another remarkable effect of the Pd cover on the Cr SDW's. With a Pd cap layer the line shape of the x-ray satellite peaks along the *K* direction (see bottom panel of Fig. 31) is smoother and more Gaussian like than for any other ferromagnetic cap layer, in particular for Fe (Fig. 12) and Co

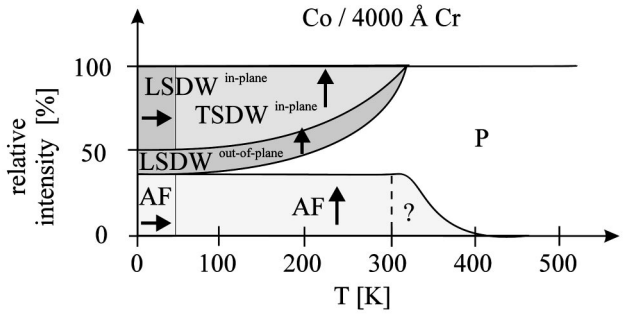

FIG. 26. Qualitative phase diagram for the commensurate and incommensurate spin-density waves in a 4000 Å thick Cr(001) film covered with a 40 Å thick Co layer, consistent with the neutron-scattering results shown in Fig. 25.

(Fig. 24). Therefore, in the Pd/Cr system less disorder appears to be present and the coherence length for the SDW's is larger than in other systems.

VI. DISCUSSION

A. Influence of overlayers

The synchrotron and neutron-scattering experiments described above provide a very clear and systematic picture of the proximity effects between the spin density waves in epitaxial Cr(001) films and magnetic or nonmagnetic cover layers. In order to work out the essential factors, we will discuss only the dominating phases observed. Let us start with an uncovered, thick Cr(001) film. In these films a single domain with a longitudinal spin-density wave propagating out-of-plane is present at low temperatures and an enhanced spin-flip transition from longitudinal to transverse is observed in the thinner of the two samples investigated.[13] Possible explanations for the out-of-plane propagation of the I-SDW and the out-of-plane orientation of the Cr spins include surface pinning effects, hybridization with the buffer Nb layer, and interaction with the native Cr-oxide layer at the surface. Deposition of a thin Cu layer on the Cr(001) surface does not change this situation very much. The spin-density wave is longitudinal and propagates out-of-plane. However, no spin flip to transverse occurs. We suspect that any other paramagnetic layer (aside from Pd) will not change these results.

As we cover the Cr(001) film with a thin Fe layer, we expect that the in-plane magnetization of the Fe layer matches the Cr spin structure, such that at the interface the Fe and Cr spins lie antiparallel, as schematically depicted in Fig. 34(a). This requires a reorientation of the spin-density wave from a longitudinal out-of-plane propagation to a transverse out-of-plane propagation with spins in the plane.

The synchrotron and neutron-scattering experiments discussed above contradict this expectation. The overriding observation for all thick Cr(001) films covered with a ferromagnetic layer (Fe,Co,Ni) is an incommensurate transverse spin-density wave, which, contrary to expectation, propagates parallel to the film plane and with spins pointing out-of-plane, perpendicular to the in-plane magnetization of the ferromagnetic films. From this observation we can immediately conclude that the specific exchange interaction between Cr and the ferromagnetic layer, which is antiferromagnetic for Fe/Cr and ferromagnetic for Co/Cr, cannot be responsible for the unexpected propagation direction of the SDW. There must be another reason.

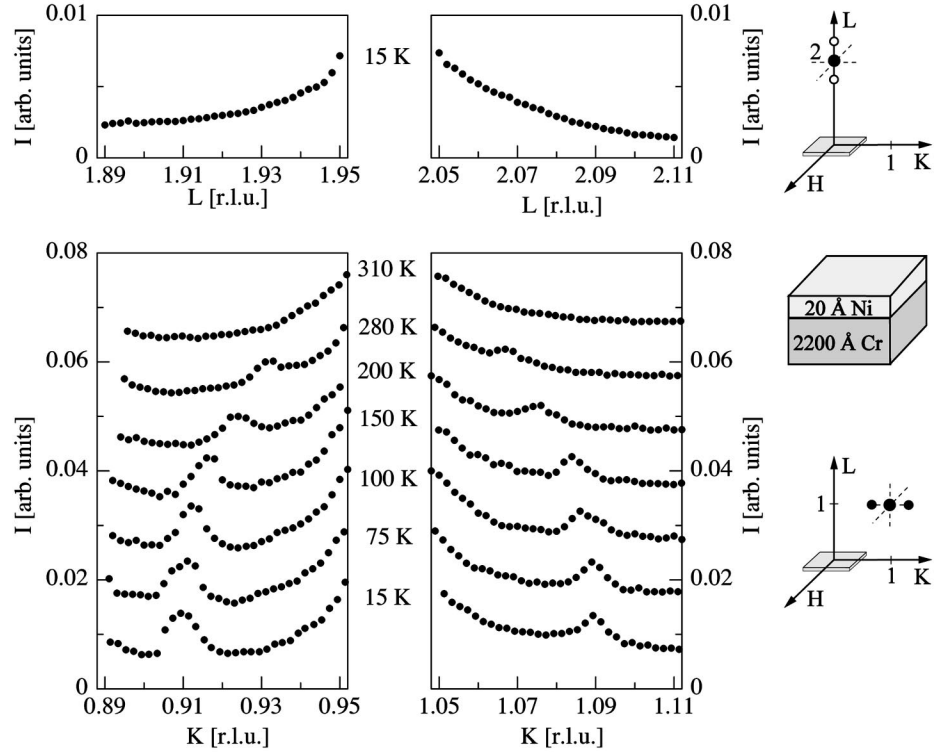

FIG. 27. Measurements with synchrotron radiation of the strain waves in a 2200 Å thick Cr(001) film covered with a 20 Å thick Ni layer. Similar to the Fe covered thick Cr films, the strain waves propagate in the film plane.

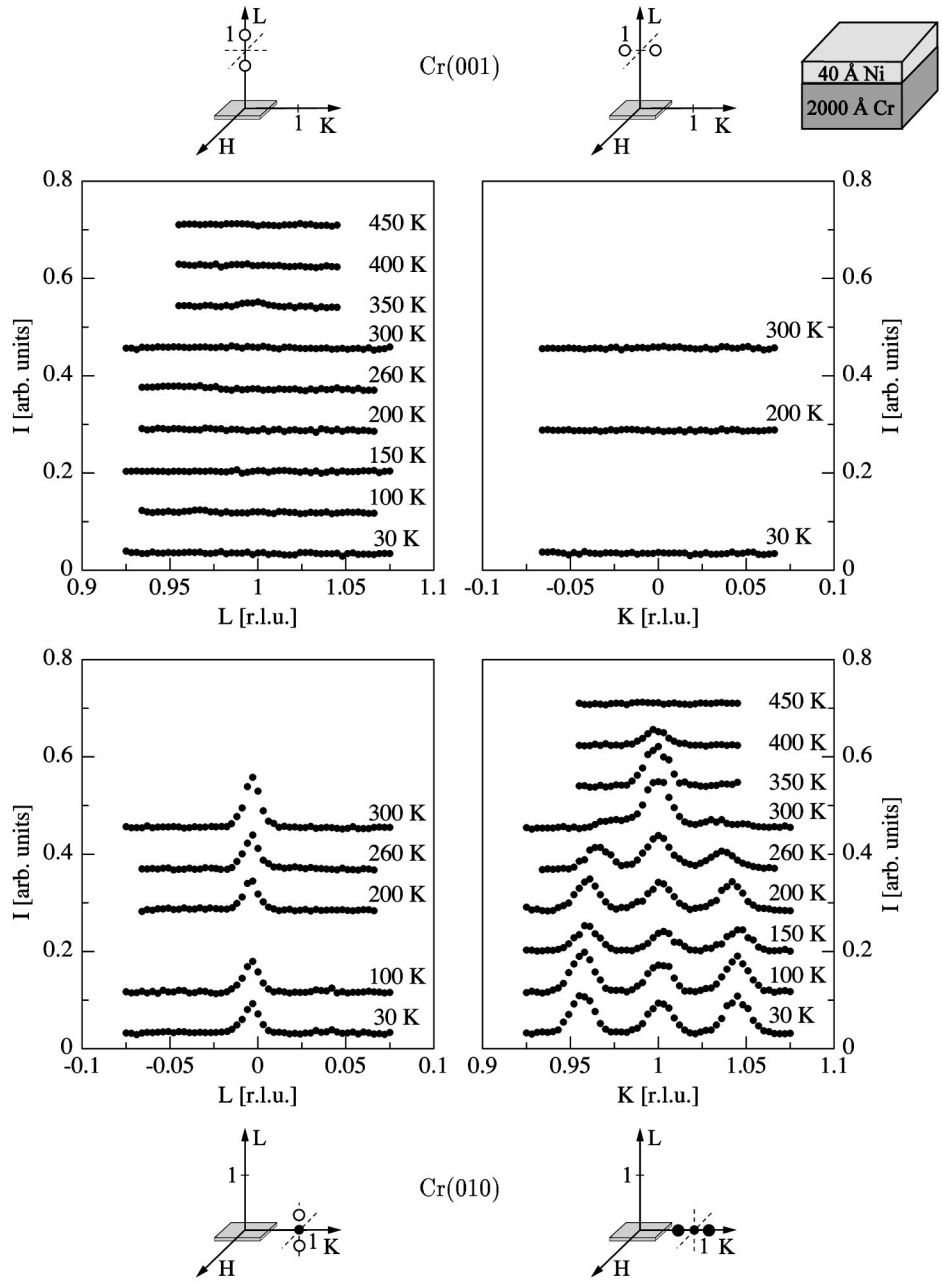

FIG. 28. Neutron-scattering experiments revealing the spin-density waves in a 2000 Å thick Cr(001) film covered with a 40 Å thick Ni layer for temperatures between 30 and 450 K. Similar to the Fe covered thick Cr films, the incommensurate spin-density wave propagates in the film plane with spins oriented out-of-plane. In addition, a commensurate phase coexists from the lowest temperature to at least 400 K.

The following discussion of Fe/Cr interface may easily be generalized to the other ferromagnetic/Cr interfaces studied. Surface roughness introduces steps of varying heights. Any step height with an odd number of atomic layers introduces frustration to the interlayer exchange coupling at the Fe/Cr interface due to the antiferromagnetic order of the Cr [see Figs. 34(b)–34(e)]. How the system overcomes this frustration depends on the relative magnitude of the intralayer exchange energies $J_{\text{Cr-Cr}}$ and $J_{\text{Fe-Fe}}$ and the interlayer exchange energy $J_{\text{Fe-Cr}}$. In case of a very small $J_{\text{Fe-Cr}}$ the frustration at the interface can be overcome by breaking the antiferromagnetic coupling at the Fe/Cr interface [Fig. 34(b)], thus avoiding the formation of domain walls in the Fe or Cr. On the other hand, in the case of a very large $J_{\text{Fe-Cr}}$ a domain wall could form either in the Fe or the Cr layer [Figs. 34(c) or 34(d)]. For an intermediate $J_{\text{Fe-Cr}}$ the system can react by forming a domain wall along the Fe/Cr interface by reorienting the Cr perpendicular to the Fe [Fig. 34(e)]. Reorientation of the Cr moments requires less energy than reorientation of the Fe moments. In the latter case work has to be done against the shape anisotropy energy, which is not required for the antiferromagnetic Cr film. Recent computer simulations using a classical Heisenberg Hamiltonian for describing the spin structure and exchange coupling for the system studied here, confirm that in the presence of steps, the Cr magnetic moments reorient in the direction perpendicular to the Fe moments[21] [Fig. 34(e)] consistent with our experimental observation. Even some interdiffusion at the interface may

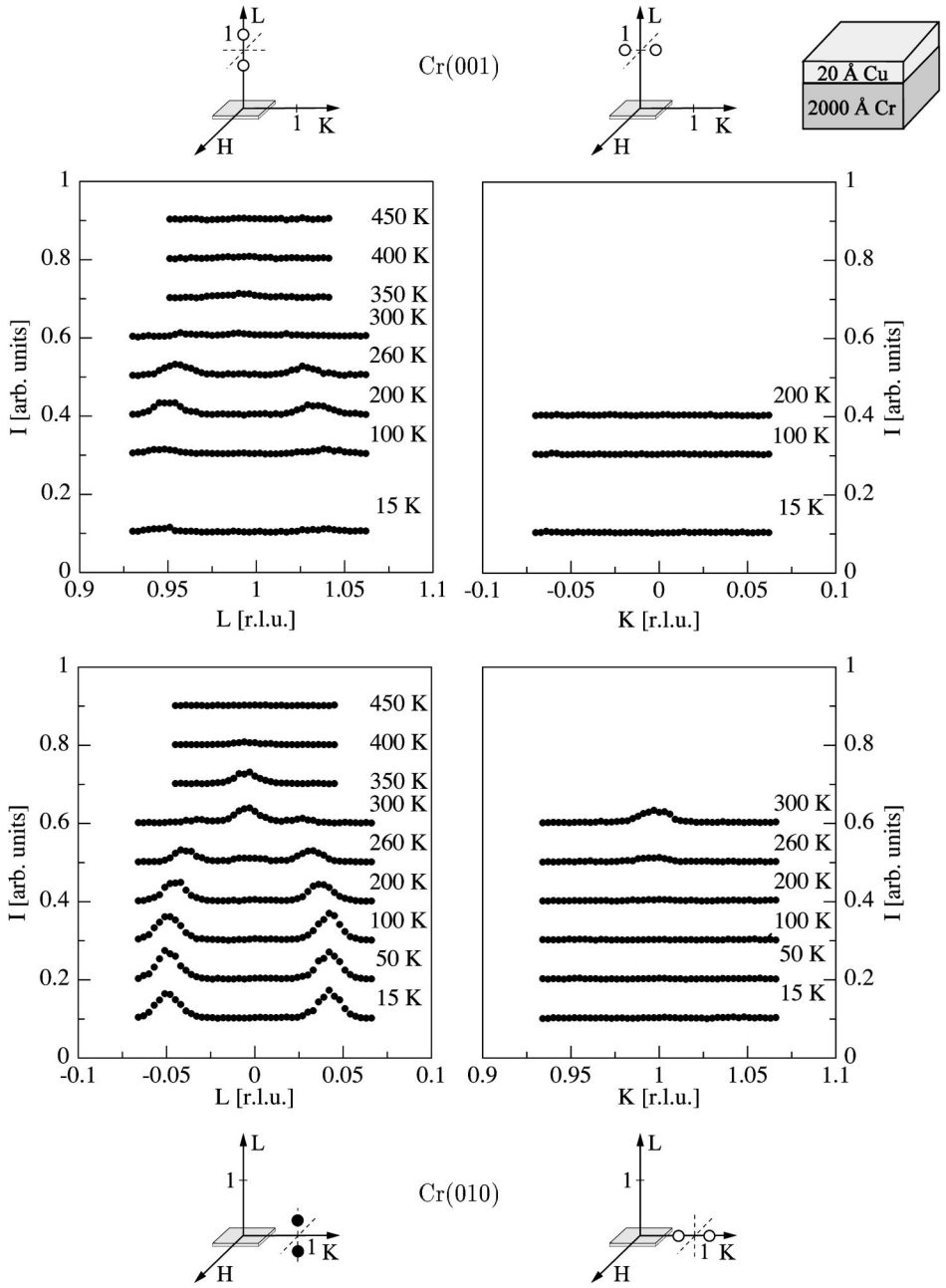

FIG. 29. Neutron-scattering experiments revealing the spin-density waves in a 2000 Å thick Cr(001) film covered with a 20 Å thick Cu layer for temperatures from 15 to 450 K. Here the incommensurate spin-density wave propagates in the out-of-plane direction and has dominantly longitudinal polarization.

be allowed without changing this conclusion. The simulation also indicates that the reorientation causes some spin disorder in the Cr spin structure close to the interface. With grazing incidence surface scattering methods, where the penetration depth of the beam can be controlled by the glancing angle of the beam to the surface, we have in fact verified this disorder.[55] The similarity of the results for all ferromagnetic overlayers implies that the above discussion is valid for Co and Ni overlayers as well.

As mentioned before, due to the high polarizability of Pd, the effect of a Pd cover on the the SDW in thick Cr(001) film is somewhere between the ferromagnetic and the uncovered case. The reorientation is only partial, such that longitudinal and transverse SDW's coexist.

Figure 33 summarizes the spin-density waves observed in thick Cr films at about 100 K and covered with different ferromagnetic and paramagnetic layers. The origin of the commensurate phase is considered in the following.

B. Origin of the commensurate spin-density waves in Cr films

There is another dominating feature of the Cr spin structure in thick films to be discussed. As soon as the transverse spin-density wave propagates in the plane, there occurs simultaneously a commensurate antiferromagnetic spin structure coexisting with the incommensurate spin-density wave. This observation can be explained as follows. A spin density wave, in order to develop, requires a structural coherence

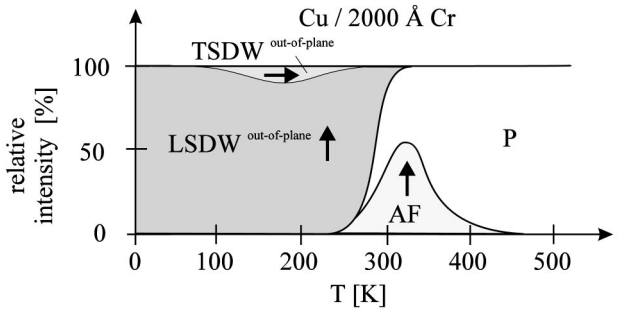

FIG. 30. Qualtitative phase diagram for the commensurate and incommensurate spin-density waves in a 2000 Å thick Cr(001) film covered with a 20 Å thick Cu layer, according to the the neutron-scattering results shown in Fig. 29.

length ξ, which is larger than roughly one period of the spin density wave, i.e. $\xi \geqslant \Lambda_{\mathrm{SDW}}$. Neutron-scattering experiments by Fullerton *et al.*[26] and Schreyer *et al.*[27] have shown that for any film thickness much smaller than Λ_{SDW}, the Cr SDW becomes commensurate. This applies also to our case. The transverse SDW in thick epitaxial Cr films, forced by the ferromagnetic cap layer combined with interfacial roughness to propagate in the plane, probes the in-plane structural coherence length $\xi_{||}$. As outlined in Sec. III A, close to the Cr/Nb interface where the misfit is large and the structural relaxation rapid, the structural coherence of the Cr film is poor. In this part of the film only a commensurate antiferromagnetic Cr spin structure can develop. Further away from the Cr/Nb interface the film quality improves significantly, i.e., $\xi_{||}$ increases, allowing a formation of an in-plane I-SDW. Recent surface neutron-scattering experiments probing the spin-density waves as a function of depth are consistent with this layering of the incommensurate and commensurate phases.[55] It should be noted that this model also holds for those samples which have a Cr/Fe/Nb growth sequence instead of Cr/Nb. Since the Fe layers are always only 20 Å thick, the Fe cannot completely relieve the strain imposed by the misfit with the Nb. Instead, the poor crystal quality will extend into the subsequent Cr layer, causing a small $\xi_{||}$, and thus a C-SDW close the Nb interface.

Vice versa, in uncovered thick Cr films the longitudinal spin-density wave propagating normal to the film plane probes the perpendicular structural coherence length $\xi_{\perp}$. Since $\xi_{\perp}$ is always much larger than $\xi_{||}$, an I-SDW can develop in these latter films. The same is also true for the Cr(001) film capped with a Cu layer.

Reviewing the phase diagrams presented above, additional C-SDW's also occur close to T_N of the I-SDW. In nearly all cases, either a new C-SDW phase occurs near T_N of the I-SDW or the intensity fraction of the existing C-SDW is enhanced considerably. Keeping in mind that Λ_{SDW} increases strongly upon approaching T_N, it is plausible to assume that a C-SDW forms whenever Λ_{SDW} is on the order of a limiting length scale.

Three different cases can be distinguished.

(1) The limiting length scale can be the film thickness t_{Cr} (for out-of plane propagation and $\xi_{\perp} = t_{\mathrm{Cr}}$), as shown experimentally by Schreyer *et al.*[27] and theoretically by Shi and Fishman.[56]

(2) For very thick films and out-of-plane propagation the limiting length scale would be $\xi_{\perp}$ instead, since then $\xi_{\perp} < t_{\mathrm{Cr}}$.

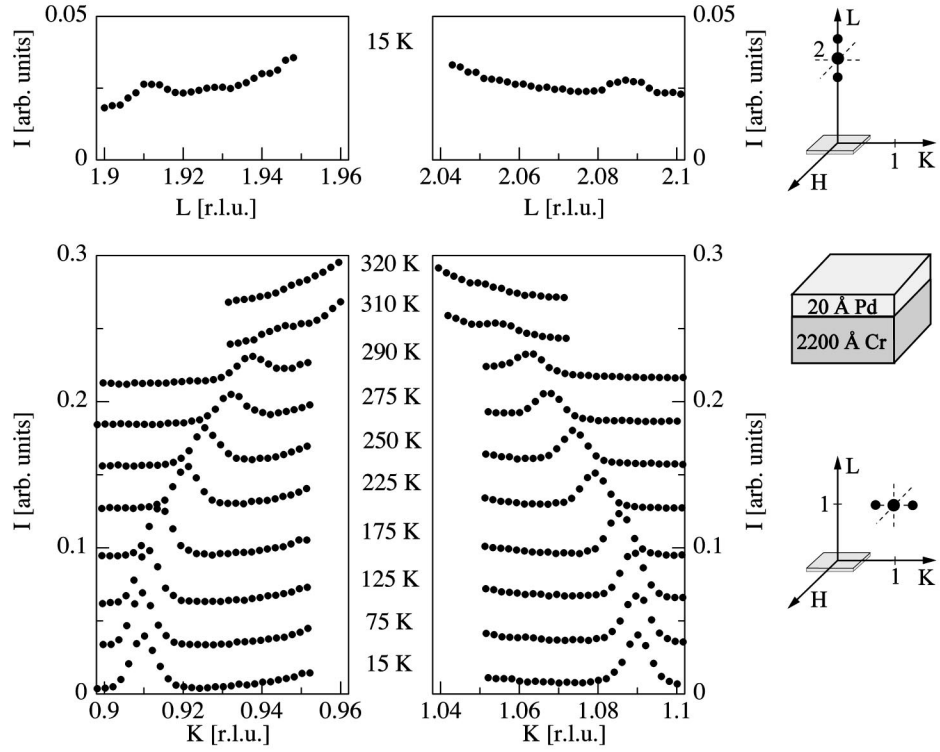

FIG. 31. Synchrotron measurements of the strain waves in a 2200 Å thick Cr(001) film capped with a 20 Å thick Pd layer. The top panel shows a scan taken at 15 K along the *L* direction across the (002) peak, the bottom panel shows scans taken at different temperatures along the *K* direction across the (110) reflection

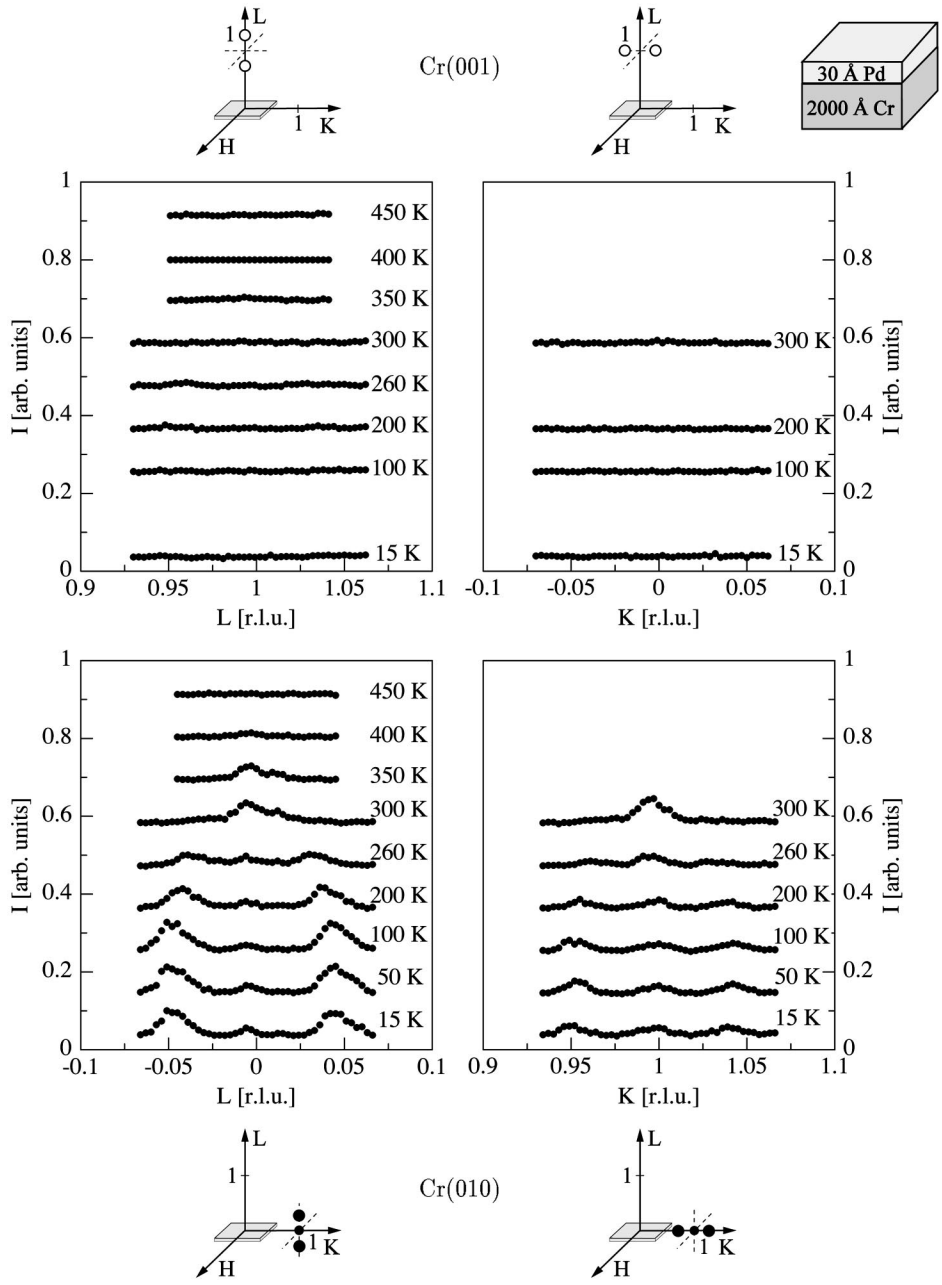

FIG. 32. Neutron-scattering experiments revealing the spin-density waves in a 2000 Å thick Cr(001) film covered with a 30 Å thick Pd layer for temperatures between 15 and 450 K. A mixture of spin-density waves can be recognized, partly with longitudinal polarization and propagating in the out-of-plane direction and partly with transverse polarization propagating in the film plane.

(3) Finally, for in-plane propagation, the limiting length scale is $\xi_{||}$.

This picture implies that in case (2) Λ_{SDW} would have to increase up to values on the order of 2000 Å which are the largest coherence lengths $\xi_{\perp}$ measured for our thickest Cr films. Such a large Λ_{SDW} may be consistent with our data, since close to T_N a strongly diverging Λ_{SDW} would lead to satellites merging into the commensurate peak position while their intensity drops dramatically.

However, an alternative explanation must be considered. It should be noted that strain is well known to cause C-SDW's in Cr.[9] Specifically, it has been found that in strained Cr powders the samples change from incommensurate into C-SDW at elevated temperatures before they become paramagnetic.[57] Therefore, the C-SDW phase occurring at high temperatures in our samples may be due to strain, induced by the large lattice misfit between the Nb buffer and the rest of the sample.

On the other hand, strain is less likely to explain the occurence of the coexisting C-SDW for in-plane propagation of the I-SDW at low temperatures. Contrary to the expectation of Poisson-like elastic behavior, x-ray measurements of the in- and out-of-plane strain in Cr(001)/Nb films as function of Cr thickness show a surprising similarity in magnitude and sign. Thus, we do not observe a drastic anisotropy between in- and out-of plane strain, whereas we do observe a drastic anisotropy in the in- and out-of-plane coherence lengths. Therefore, we attribute the occurrence of the C-SDW for in-plane I-SDW propagation to the anisotropy in the in- and out-of-plane coherence lengths as the dominating factor. Al-

though we cannot exclude the significance of strain effects it should be noted that in any case the large lattice misfit at the Cr/Nb interface is the underlying cause of these C-SDW's. Finally, for small Cr thicknesses the strong t_{Cr} dependence of the phenomena indicates, that the limiting length scale t_{Cr}, not strain at the Cr/Nb interface, is the important parameter determining the existence of a C-SDW in our samples.

In conclusion, the presence of C-SDW's in our samples can be explained by strain as well as finite-size effects induced by the limiting length scales $t_{Cr}, \xi_{\perp}$, or $\xi_{||}$, depending on the propagation direction of the I-SDW.

C. Film thickness dependence

Next we discuss the dependence of the spin-density waves on the Cr film thickness. Systematic studies are only available for Cr(001) films covered with Fe layers. However, we expect similar behavior for any ferromagnetic/Cr interface.

As the Cr film thickness is reduced, we observe a reorientation of the I-SDW from propagating parallel to the film plane to normal to the film plane. This reorientation starts at a Cr film thickness of about 1000 Å, and is finished at 250 Å. Between 250 and about 45 Å there is only a single transverse I-SDW propagating normal to the film plane and with spins in the plane. This is the situation which we expected in the beginning and which is schematically depicted in Fig. 23.

The reorientation of the spin-density wave indicates that with decreasing thickness more energy is gained by forming domain walls in the Cr [Fig. 34(d)] than by forming a 90° wall along the Fe/Cr interface [Fig. 34(e)]. The case of domain walls in the Fe [Fig. 34(c)], which would lead to a vanishing magnetization of the Fe layers, is not observed experimentally. Since the energy gained by domain-wall formation in the Cr film scales with the Cr film thickness t_{Cr}, while the energy gained by reorienting the Cr moments perpendicular to the Fe/Cr interface scales with the separation $\mathcal{L}$ of the steps and kinks at the interface, we expect that the crossover from out-of-plane to in-plane spin orientation takes place roughly when the condition $J_{Cr\text{-}Cr} \times t_{Cr} = J_{Fe\text{-}Cr} \times \mathcal{L}$ is fullfilled, where $J_{Cr\text{-}Cr}$ and $J_{Fe\text{-}Cr}$ are the Cr-Cr and Fe-Cr exchange energies, respectively. Computer simulations of the Cr spin structure with a rough Fe/Cr interface confirm this estimate.[21,58] Since the $J_{Cr\text{-}Cr}$ and $J_{Fe\text{-}Cr}$ exchange energies are roughly on the same order of magnitude, we expect a reorientation at a film thickness of $t_{Cr} \approx \mathcal{L}$. X-ray-scattering experiments on the interfacial roughness of similarly prepared Fe/Cr interfaces confirm this estimate.[24] If the Cr film thickness is reduced well below the period Λ_{SDW} of the SDW, the SDW state collapses due to finite-size effects and Cr becomes commensurate antiferromagnetic, accomodating the frustration due to the interface structure by spirals of opposing sense of rotation.[27] In Fig. 35 the spin-density-wave states in epitaxial Cr(001) films covered with a ferromagnetic Fe layer are qualitatively summarized as a function of the Cr film thickness, reproducing the situation present at a temperature of about 100 K. The data for the thinnest samples from Ref. 27 have been added for completeness.

A striking feature of the phase diagram is that upon reorientation of the transverse I-SDW from in-plane to out-of-plane propagation the concomitant C-SDW vanishes completely. As outlined in the previous section, this behavior is the result of a strong anisotropy in the crystalline in-plane and out-of-plane coherence lengths.

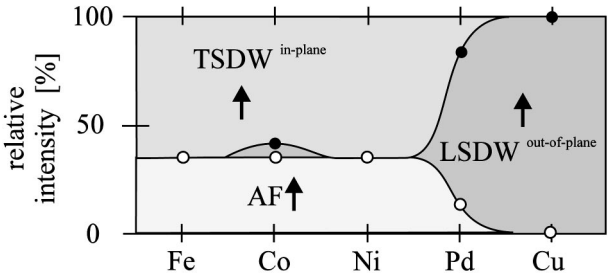

FIG. 33. Phase diagram for spin-density waves in about 3000 Å thick Cr(001) films covered with different ferromagnetic and paramagnetic thin layers. The phase diagram reflects the situation observed at about 100 K. The arrows indicate the orientation of the Cr magnetic moments, where the vertical orientation refers to the out-of-plane direction.

VII. SUMMARY

In summary, we have presented extensive synchrotron x-ray and neutron-scattering results probing the spin-density waves in epitaxial Cr(001) films. In particular, we have studied the effect of ferromagnetic and paramagnetic thin cap layers on the spin-density-wave state in the Cr. With a 20-Å-thick ferromagnetic Fe cap layer and varying Cr film thickness, the scenario for the proximity effect between the ferromagnetic and spin-density-wave state can be described as follows. For large Cr film thicknesses and a perfect Fe/Cr interface without roughness a single incommensurate transverse SDW with propagation out-of-the plane and spins in the plane is expected. Instead, we observe an incommensurate transverse SDW propagating in the film plane with spins pointing out-of-plane at a right angle to the in-plane magnetization of the cap ferromagnetic layer. The incommensurate SDW coexists with a commensurate SDW starting already at the lowest temperatures investigated. In the commensurate phase the spins have the same out-of-plane spin orientation as in the incommensurate phase. The incommensurate phase exhibits a Néel temperature essentially identical with the bulk Néel temperature, whereas the transition from the commensurate antiferromagnetic structure to the paramagnetic state occurs at much higher temperatures of about 450 K. The Cr spin structure in relation to the ferromagnetic cap layer can be understood in terms of interfacial roughnesses, causing frustrations of the exchange coupling at the interface, which in turn causes a reorientation of the Cr moments. As the Cr film thickness is decreased, energy gain from forming domain walls in the Cr begins to dominate the reorientation effect and the Cr spins start to align parallel to the ferromagnetic layer. When this procedure is finished at a Cr thickness of about 250 Å, the incommensurate SDW propagates perpendicular to the film plane with spins oriented parallel to the film plane. During this rotation of the I-SDW the C-SDW phase vanishes. Finally, when the Cr film thickness becomes much smaller than the period of the incommensurate SDW, the SDW collapses and the Cr film becomes commensurate antiferromagnetic with a Néel temperature of 500 K, i.e., somewhat higher than in the commensurate state dis-

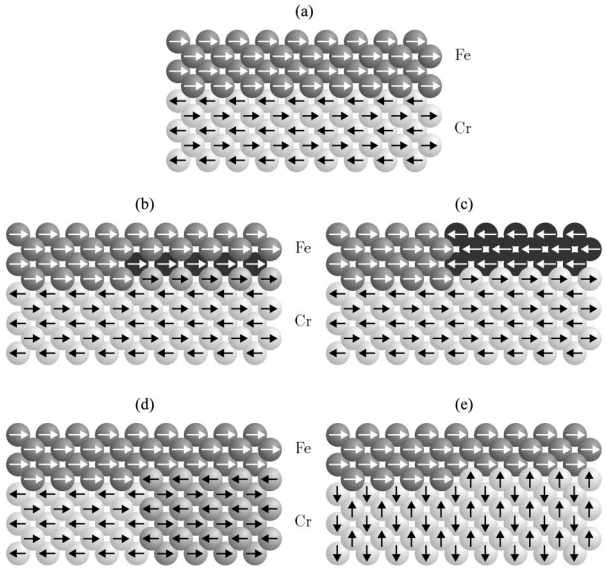

FIG. 34. Schematic and simplified representation of the interface between a thin ferromagnetic Fe layer and a thicker antiferromagnetic Cr film. The white arrows indicate the orientation of the magnetic moments in the Fe film, the black arrows the Cr magnetic moments. (a) represents an ideal and flat interface with antiferromagnetic coupling between the Fe and Cr moments. (b)–(e) show interfaces with monoatomic high steps causing frustration of the interface exchange coupling. The frustration can be overcome be formation of a domain in the Fe layer (c), in the Cr film (d), or by a reorientation of the spin-density wave (e). The latter case is observed experimentally in thick Cr films.

cussed before.[59] Fe, Co, and Ni cap layers have the same effect on the propagation of the SDW in Cr, although the interface exchange coupling may be opposite, i.e., antiferromagnetic in the case of Fe/Cr and ferromagnetic in the case of Co/Cr. A cap layer of Cu on Cr has essentially the same effect on the SDW's as a Cr/vacuum or a Cr/Cr_2O_3 interface. In either case we observe a dominant longitudinal SDW propagating normal to the film plane. The effect of a Pd cap layer on Cr is different from other paramagnetic cap layers. Due to the high polarizability, Pd behaves as a weak ferromagnet causing a a partial rotation of the SDW. Thus in Pd-capped Cr films, longitudinal out-of-plane and transverse in-plane SDW's coexist.

The occurrence of the commensurate phase can be attributed to strain and finite-size effects. In the latter case the Cr film thickness or the in- or out-of-plane crystalline coherence lengths determine if an I-SDW can form a complete period, i.e., remain incommensurate.

From a practical point of view our experiments show that single-domain spin-density waves in Cr can easily be produced without the application of external magnetic fields or mechanical stresses. A longitudinal incommensurate spin-

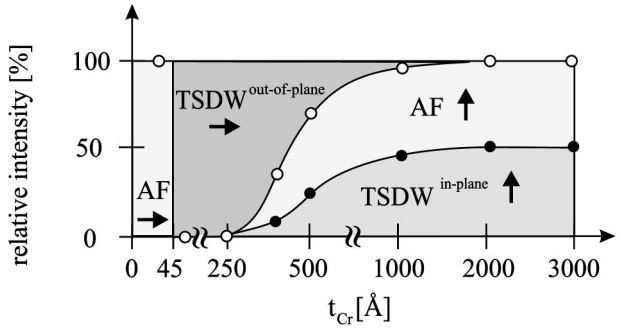

FIG. 35. Qualitative phase diagram of the spin-density waves in epitaxial Cr(001) films covered with thin a Fe layer as a function of the Cr film thickness. The phase diagram represents the situation at about 100 K. The arrows indicate the orientation of the Cr magnetic moment, where the vertical direction corresponds to spins oriented perpendicular to the film plane.

density wave propagating normal to the film is present in epitaxial Cr(001) films of 500–2000 Å thickness, capped either with a native oxide layer or with a paramagnetic layer of low polarizability. A transverse I-SDW propagating in the film plane can be generated in Cr(001) films of about 3000 Å thickness when covered with a ferromagnetic layer. Finally, a transverse I-SDW propagating in the out-of-plane direction is present in thin Cr(001) films of less than 250 Å covered again with a ferromagnetic layer. Commensurate SDW's can be obtained by limiting the Cr thickness or crystalline coherence lengths to values well below Λ_{SDW}, or by increasing the temperatures to values above T_N of the I-SDW.

All the foregoing results lead us to the final and important conclusion that the spin-density waves in epitaxial Cr(001) films can easily be manipulated in a systematic and predictable fashion by the choice of the magnetic cover, the interfacial roughness, and the chromium film thickness.

ACKNOWLEDGMENTS

We would like to acknowledge the fruitful contributions of P. Sonntag and the collaborations with our co-workers at the different neutron and synchrotron facilities where we have collected our data, in particular J. Borchers and C.F. Majkrzak at NIST, K. Hamacher and H. Kaiser at MURR, D. Gibbs, B. Ocko, and T. Thurston, at NSLS, and F. Güthoff and G. Eckold at Jülich. This work was supported by the Deutsche Forschungsgemeinschaft through SFB 166 (''Strukturelle und magnetische Phasenumwandlungen''), by the Ministerium fr Wissenschaft und Forschung NRW, and by NATO through travel Grant No. CRG901064. H.Z. and A.S. also acknowledge financial support from the Volkswagen and Alexander von Humboldt foundations, respectively, while this manuscript was written.

[1] L. M. Corliss, J. M. Hastings, and R. J. Weiss, Phys. Rev. Lett. **3**, 211 (1959).

[2] G. Binasch, P. Grünberg, F. Saurenbach, and W. Zinn, Phys. Rev. B **39**, 4828 (1989).

[3] M. N. Baibich, J. M. Broto, A. Fert, F. Nguyen Van Dau, F. Petroff, P. Etienne, B. Greuzet, A. Friederich, and J. Chazelas, Phys. Rev. Lett. **61**, 2472 (1988).

[4] C. T. Yu, K. Westerholt, K. Theis-Bröhl, V. Leiner, Th. Zeidler, and H. Zabel, Phys. Rev. B **37**, 2955 (1998).

[5] S. Blügel, D. Pescia, and P. H. Dederichs, Phys. Rev. B **39**, 1392 (1989).

[6] R. Wiesendanger, H.-J. Güntherodt, G. Güntherodt, R. J.

Gambino, and R. Ruf, Phys. Rev. Lett. **65**, 247 (1990).
[7] J. Meerschaut, J. Dekoster, R. Schad, P. Beliën, and M. Rots, Phys. Rev. Lett. **75**, 1638 (1995).
[8] J. Meerschaut, J. Dekoster, S. Demuynck, S. Cottenier, B. Swinnen, and M. Rots, Phys. Rev. B **57**, 5575 (1998).
[9] E. Fawcett, Rev. Mod. Phys. **60**, 209 (1988).
[10] A. Arrott, S. A. Werner, and H. Kendrick, Phys. Rev. **153**, 624 (1967).
[11] E. Fawcett, L. Alberts, V. Y. Galkin, D. R. Noakes, and J. V. Yakhmi, Rev. Mod. Phys. **66**, 25 (1994).
[12] P. Sonntag, P. Bödeker, T. Thurston, and H. Zabel, Phys. Rev. B **52**, 7363 (1995).
[13] P. Sonntag, P. Bödeker, A. Schreyer, H. Zabel, K. Hamacher, and H. Kaiser, J. Magn. Magn. Mater. **183**, 5 (1998).
[14] R. Jungblut, Ch. Roth, F. U. Hillebrecht, and E. Kisker, J. Appl. Phys. **70**, 5923 (1990).
[15] J. Unguris, R. J. Cellotta, and D. T. Pierce, Phys. Rev. Lett. **67**, 140 (1991).
[16] J. Unguris, R. J. Celotta, and D. T. Pierce, Phys. Rev. Lett. **69**, 1125 (1992).
[17] D. Stoeffler and F. Gautier, J. Magn. Magn. Mater. **147**, 260 (1995); A. Vega *et al.*, Europhys. Lett. **31**, 561 (1995); M. Freyss, D. Stoeffler, and H. Dreyssee, Phys. Rev. B **56**, 6047 (1997).
[18] C. Turtur and G. Bayreuther, Phys. Rev. Lett. **72**, 1557 (1994).
[19] P. Bödeker, P. Sonntag, A. Schreyer, J. Borchers, K. Hamacher, H. Kaiser, and H. Zabel, J. Appl. Phys. **81**, 5247 (1997).
[20] P. Bödeker, P. Sonntag, A. Schreyer, H. Zabel, J. Borchers, K. Hamacher, and H. Kaiser, Physica B **234-236**, 464 (1997).
[21] P. Bödeker, A. Hucht, J. Borchers, F. Güthoff, A. Schreyer, and H. Zabel, Phys. Rev. Lett. **81**, 914 (1998).
[22] H. Zabel, A. Schreyer, P. Bödeker, and P. Sonntag, in *Spin Density Waves and Proximity Effects in Thin Epitaxial Cr Films*, in *Dynamical Properties of Unconventional Magnetic Systems*, edited by A. T. Skjeltorp and D. Sherrington, NATO ASI Series E: Applied Sciences, Vol. 349 (Kluwer Academic, Dordrecht, 1998).
[23] H. Zabel, P. Bödeker, and A. Schreyer, J. Phys. D **31**, 656 (1998).
[24] A. Schreyer, J. F. Ankner, Th. Zeidler, H. Zabel, M. Schäfer, J. A. Wolf, P. Grünberg, and C. F. Majkrzak, Phys. Rev. B **52**, 16 066 (1995); Europhys. Lett. **32**, 595 (1995).
[25] E. E. Fullerton, K. T. Riggs, C. H. Sowers, S. D. Bader, and A. Berger, Phys. Rev. Lett. **75**, 330 (1995).
[26] E. E. Fullerton, S. D. Bader, and J. L. Robertson, Phys. Rev. Lett. **77**, 1382 (1996).
[27] A. Schreyer, C. F. Majkrzak, Th. Zeidler, T. Schmitte, P. Bödeker, K. Theis-Bröhl, A. Abromeit, J. Dura, and T. Watanabe, Phys. Rev. Lett. **79**, 4914 (1997).
[28] E. E. Fullerton, C. H. Sowers, and S. D. Bader, Phys. Rev. B **56**, 5468 (1997).
[29] S. A. Werner, A. Arrott, and H. Kendrick, Phys. Rev. **155**, 528 (1967).
[30] Y. Tsunoda, M. Mori, N. Kunitomi, Y. Teraoka, and J. Kanamori, Solid State Commun. **14**, 287 (1974).
[31] D. Gibbs, K. M. Mohanty, and J. Bohr, Phys. Rev. B **37**, 562 (1988).
[32] J. P. Hill, G. Helgesen, and D. Gibbs, Phys. Rev. B **51**, 10 336 (1995).
[33] A. Arrott, in *Magnetism*, edited by G. Rado and H. Suhl (Academic, New York, 1966), Vol. IIB, p. 295.
[34] S. W. Lovesey, *Theory of Neutron Scattering from Condensed Matter* (Clarendon, Oxford, 1984).
[35] J. P. Hill, C. C. Kao, and D. F. McMorrow, Phys. Rev. B **55**, R8662 (1997).
[36] Th. Brückel, M. Lippert, R. Bouchard, T. Schmidt, J. R. Schneider, and W. Jauch, Acta Crystallogr., Sect. A: Found. Crystallogr. **49**, 679 (1993).
[37] M. Lippert, Th. Brückel, T. Köhler, and J. R. Schneider, Europhys. Lett. **27**, 537 (1994); J. Strempfer, Th. Brückel, D. Hupfeld, and J. R. Schneider, *ibid.* **40**, 569 (1997).
[38] S. M. Durbin, J. A. Cunningham, M. E. Mochel, and C. P. Flynn, J. Phys. F **11**, L223 (1981); **12**, L75 (1982); **15**, L221 (1985).
[39] K. Theis-Bröhl, I. Zoller, P. Bödeker, H. Zabel, L. Brendel, M. Belzer, and D. E. Wolf, Phys. Rev. B **57**, 4747 (1998).
[40] P. Sonntag, W. Donner, N. Metoki, and H. Zabel, Phys. Rev. B **49**, 2869 (1994).
[41] R. People and J. C. Bean, Appl. Phys. Lett. **47**, 322 (1985).
[42] A. Stierle and H. Zabel, Europhys. Lett. **37**, 365 (1997).
[43] Th. Zeidler, F. Schreiber, H. Zabel, W. Donner, and N. Metoki, Phys. Rev. B **53**, 3256 (1996).
[44] A. Berger and H. Hopster, Phys. Rev. Lett. **73**, 193 (1994).
[45] A. W. Overhauser, Phys. Rev. **128**, 1437 (1962).
[46] I. S. Williams and R. Street, Philos. Mag. B **43**, 955 (1981).
[47] Ko Mibu, S. Tanaka, and T. Shinjo (unpublished).
[48] S. Demuynck, J. Meerschaut, J. Dekoster, B. Swinnen, R. Moons, A. Vantomme, S. Cottenier, and M. Rots, Phys. Rev. Lett. **81**, 2562 (1998).
[49] W. Donner, N. Metoki, A. Abromeit, and H. Zabel, Phys. Rev. B **48**, 14 745 (1993).
[50] W. Donner, Th. Zeidler, F. Schreiber, N. Metoki, and H. Zabel, J. Appl. Phys. **75**, 6421 (1994).
[51] N. Metoki, W. Donner, and H. Zabel, Phys. Rev. B **49**, 17 351 (1994).
[52] F. Schreiber, Z. Frait, Th. Zeidler, N. Metoki, W. Donner, H. Zabel, and J. Pelzl, Phys. Rev. B **51**, 2920 (1995).
[53] *Magnetic Properties of Metals, d-Elements, Alloys and Compounds*, Data in Science and Technology, edited by H. P. J. Wijn (Springer-Verlag, Berlin, 1991).
[54] S. Blügel and P. H. Dederichs, Europhys. Lett. **9**, 597 (1989).
[55] P. Bödeker, A. Schreyer, P. Sonntag, Ch. Sutter, G. Grübel, and H. Zabel, Physica B (to be published).
[56] Z. P. Shi and R. S. Fishman, Phys. Rev. Lett. **78**, 1351 (1997).
[57] I. S. Williams and R. Street, Philos. Mag. B **43**, 893 (1981).
[58] A. Hucht (private communication); (unpublished).
[59] T. Schmitte, A. Schreyer, P. Bödeker, and H. Zabel (unpublished).